British Geological Survey
NATURAL ENVIRONMENT RESEARCH COUNCIL

FENAC
FACILITY FOR ENVIRONMENTAL NANOSCIENCE ANALYSIS AND CHARACTERISATION

Sampling and characterising groundwater nanoparticles in sub-oxic environments

Groundwater Science Programme

Internal Report IR/11/021

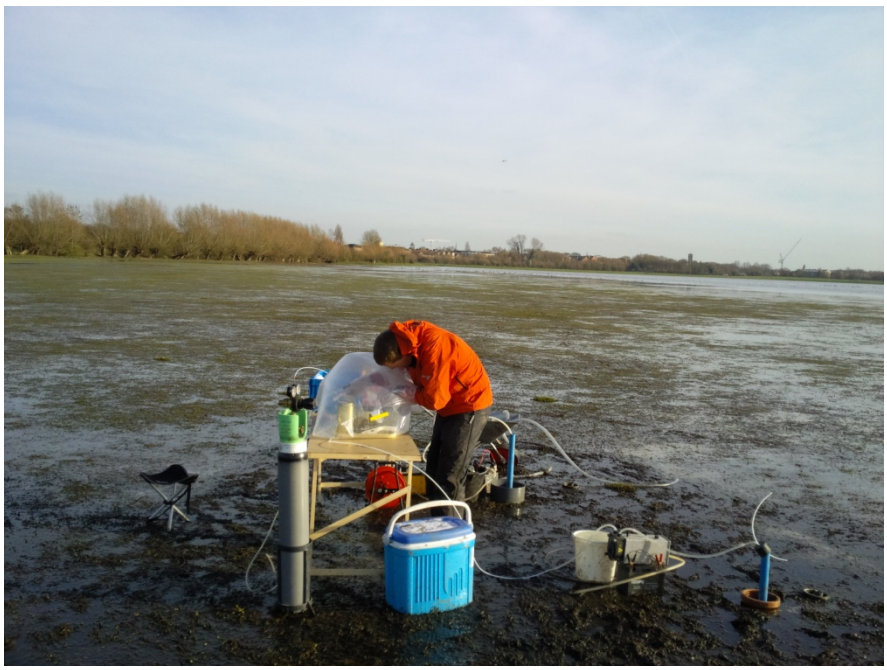

BRITISH GEOLOGICAL SURVEY

GROUNDWATER SCIENCE PROGRAMME

INTERNAL REPORT IR/11/021

Sampling and characterising groundwater nanoparticles in sub-oxic environments

D J Lapworth, B Stolpe, D C Gooddy and J R Lead

Keywords

Groundwater, nanoparticle characterisation, sub-oxic, anaerobic environments.

Front cover

Sampling nanoparticles at site PTM28, Port Meadow, Oxford.

Bibliographical reference

LAPWORTH D J, STOLPE B, GOODDY D C AND LEAD J R. 2011. Sampling and characterising groundwater nanoparticles in sub-oxic environments. *British Geological Survey Internal Report*, IR/11/021. 40pp.

Keyworth, Nottingham British Geological Survey 2011

BRITISH GEOLOGICAL SURVEY

The full range of our publications is available from BGS shops at Nottingham, Edinburgh, London and Cardiff (Welsh publications only) see contact details below or shop online at www.geologyshop.com

The London Information Office also maintains a reference collection of BGS publications, including maps, for consultation.

We publish an annual catalogue of our maps and other publications; this catalogue is available online or from any of the BGS shops.

The British Geological Survey carries out the geological survey of Great Britain and Northern Ireland (the latter as an agency service for the government of Northern Ireland), and of the surrounding continental shelf, as well as basic research projects. It also undertakes programmes of technical aid in geology in developing countries.

The British Geological Survey is a component body of the Natural Environment Research Council.

British Geological Survey offices

BGS Central Enquiries Desk

Tel 0115 936 3143 Fax 0115 936 3276

email enquiries@bgs.ac.uk

Environmental Science Centre, Keyworth, Nottingham NG12 5GG

Tel 0115 936 3241 Fax 0115 936 3488

email sales@bgs.ac.uk

Murchison House, West Mains Road, Edinburgh EH9 3LA

Tel 0131 667 1000 Fax 0131 668 2683

email scotsales@bgs.ac.uk

Natural History Museum, Cromwell Road, London SW7 5BD

Tel 020 7589 4090 Fax 020 7584 8270

Tel 020 7942 5344/45 email bgslondon@bgs.ac.uk

Columbus House, Greenmeadow Springs, Tongwynlais, Cardiff CF15 7NE

Tel 029 2052 1962 Fax 029 2052 1963

Maclean Building, Crowmarsh Gifford, Wallingford OX10 8BB

Tel 01491 838800 Fax 01491 692345

Geological Survey of Northern Ireland, Colby House, Stranmillis Court, Belfast BT9 5BF

Tel 028 9038 8462 Fax 028 9038 8461

www.bgs.ac.uk/gsni/

Parent Body

Natural Environment Research Council, Polaris House, North Star Avenue, Swindon SN2 1EU

Tel 01793 411500 Fax 01793 411501

www.nerc.ac.uk

Website www.bgs.ac.uk

Shop online at www.geologyshop.com

Acknowledgements

Funding for nanoparticle characterisation came from a FENAC grant (FENAC/2009/12/001). Fieldwork and other analysis was funded through the BGS Groundwater Processes team, part of the Groundwater Science Programme of BGS. The authors acknowledge the assistance of Kate Griffiths and Peter Williams (BGS) in the collection of groundwater samples. The authors thank Oxford County Council for allowing access to the field site.

Contents

FIGURES

PLATES

TABLES

Summary

Characterising nanoparticles is important for understanding physiochemical and biogeochemical processes occurring within groundwater bodies e.g. those impacted by the migration of leachates from waste storage sites as well as monitoring the use of engineered nanotechnology for pollution attenuation. While characterising nano-scale particles (both natural and engineered) within sub-oxic environments is a challenging task, it is critical for understanding pollution attenuation and migration within a number of different environments. The overall aim of this study was to develop a robust sampling and analytical methodology for characterising nanoparticles in sub-oxic environments using a range of complementary methods.

This study has successfully sampled and characterised nano-scale particulate material in sub-oxic groundwaters within an alluvial floodplain aquifer impacted by a landfull plume. The integrity of the sample was maintained throughout the field and laboratory work to ensure that only nanoparticles representative of the sub-oxic environment were characterised. Nanoparticles from two pairs of nested boreholes were characterised by a number of state-of-the-art methods; atomic force microscopy (AFM), scanning electron microscopy (SEM), scanning transmisson electron microscopy (TEM) and field flow fractionation (FFF), to explore particle size distributions, morphology and surface chemistry. It is important to characterise nanoparticles in environmental contexts using multiple techniques as each method has its own benefits and limitations (Lead and Wilkinson 2006). As far as the authors are aware this is the first such study in the UK to isolate and characterise sub-oxic groundwater nanoparticles using these complimentary techniques.

Groundwaters were found to have abundant iron and organic nanoparticles with diameters <30 nm. AFM results showed spherical nanoparticles with average diameters of ca 10 nm, while FFF with UV absorbance (254 nm) results indicated that smaller fulvic-like nanoparticles were present with average hydrodynamic diameters of ca. 1.5 nm. FFF with UV absorbance detection at 575 nm showed that another population of organic rich nanoparticles was present with larger hydrodynamic diameters (ca. 3 nm) in the groundwater at nest 26, but were not present in nest 28. These larger organic nanoparticles perhaps represent co-aggregated humic-like particles or another distinct type of organic matter. Scanning TEM analysis with energy-dispersive X-ray diffraction showed that Ca rich nanoparticles were present within the groundwater at a number of sites, and that P was associated with the surface of Fe rich particles in nest 28.

Aeration of sub-oxic samples resulted in a dramatic shift in the nanoparticle size distribution. This was a result of the aggregation of smaller nanoparticles to form larger agglomerations with diameters typically >50-100 nm. This is analogous to processes that occur during groundwater aeration for water treatment, and mixing of anaerobic and aerobic environmental waters, e.g. during rapid recharge events, flooding, hyporheic zone mixing, waste water treatment and waste water inputs to surface waters.

The techniques developed in this study have potential wider applications for understanding the occurrence and fate of natural and anthropogenic (engineered) nanoparticles in sub-oxic conditions, such as the fate of nanoparticles injected for pollution attenuation, those found below landfill sites, within waste water treatment works and the hyporheic zone which are all important redox hot-spots for pollution attenuation and biological activity.

1 Introduction

Natural nanoparticles (i.e. particles with one dimension less than 100 nm) and colloidal material (particles with one dimension between 1 nm and 1μm), such as iron or silica mineral particles, complex organic molecules such as humic-like substances, or material derived from bacterial sources are important vectors for contaminants (Grolimund et al., 1996; Degueldre et al., 2000; Klaine et al., 2008). The formation of these particles can enhance the mobility of otherwise immobile contaminants providing a pathway for groundwater and river water pollution (Lead and Wilkinson, 2006). Conversely, natural nanoparticles can also attenuate contaminant transport in some cases, and are known to have an important role in biogeochemical cycling, and bioavailability of nutrients and toxic substances (e.g Waychunas et al., 2005; Speelmans et al., 2007).

There has been a significant body of research in recent years on the use (reductive properties) of manufactured nanoparticles for contaminant attenuation and remediation of groundwater (Elliot and Zhang, 2001; Zhang, 2003, Schrick et al., 2004, Lui et al, 2005, Sohn et al, 2006, Giasuddin et al, 2007, Reinsch et al., 2010). Research on characterising groundwater nanoparticles has also focussed on understanding radionuclide fate and transport (e.g. Bargar et al., 2008, Utsunomiya et al., 2009). Wolthoorn et al. (2004a, 2004b) used scanning electron microscopy (SEM-EDX) to characterised Fe colloids following artificial groundwater aeration for in-situ Fe removal in anaerobic groundwaters.

To date very few published studies have successfully sampled and characterised nanoparticles in anaerobic groundwaters using modern state-of-the-art techniques namely, field flow field fractionation (FFF), atomic force microscopy (AFM), transmission electron microscopy (TEM) and environmental scanning electron microscopy (SEM). This is due to only relatively recent developments in analytical methods (e.g. Balnois et al., 1999, Lead et al., 2005, Redwood et al., 2005, Baalousha and Lead 2007) and the challenges in collecting a representative sample from anaerobic waters. In light of this a collaborative project between BGS and NERC's Facility for Environmental Nanoparticle Characterisation (FENAC) was initiated with the focus to develop a reliable method for sampling and characterising nanoparticles in anaerobic groundwaters. This method will be of relevance to a wide range of environmental studies investigating the fate and transport of nanoparticles and contaminant mobility/attenuation in anaerobic environmental conditions.

2 Study site

Figure 1 shows a map of the site, known as Port Meadow, located on the Thames floodplain in a peri-urban setting, between west Oxford and the River Thames. The study site for this project is classed as a Sites of Special Scientific Interest (SSSI), and is also a Special Area of Conservation (SAC) with internationally important lowland hay meadow habitats (Gowing and Youngs, 2005). This area has a series of boreholes completed in the underlying sands and gravels and bedrock to monitor the groundwater chemistry and temporal water level fluctuations. This site is being used as an environmental observatory for a number of different NERC and externally funded projects as part of the BGS groundwater science programme investigating amongst other things groundwater flooding, biogeochemical cycling and pollution attenuation in peri-urban floodplain environments (Macdonald et al., 2007, Griffiths et al., 2011). Up gradient of the borehole nests (26 and 28) there is an area of made ground that was a former land fill site which was capped in the 1980's.

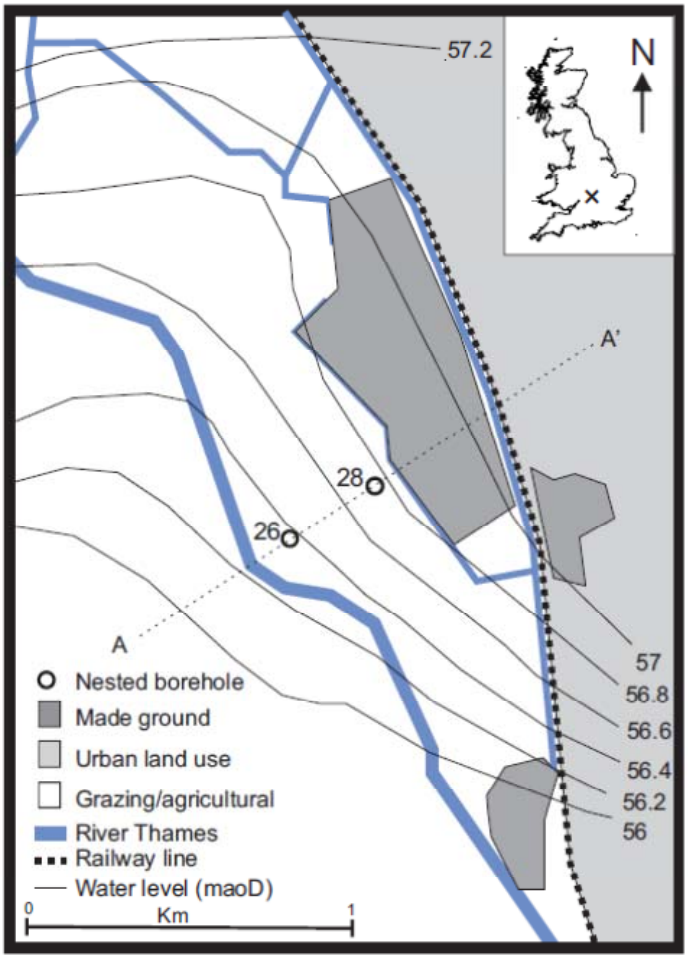

Figure 1 Location of study site for groundwater sampling on Port Medeaw, Oxford. A-A'is the section for Figure 2.

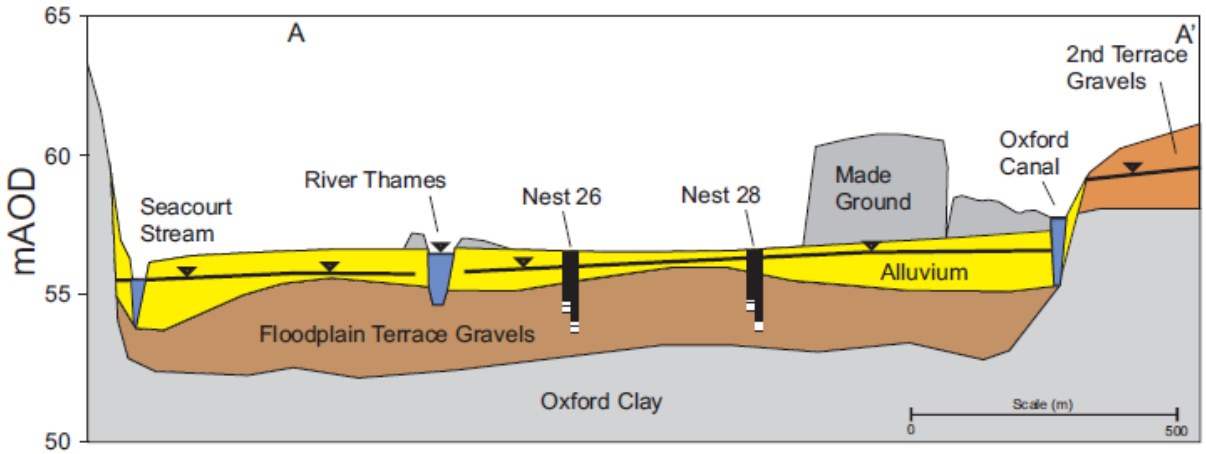

Figure 2 Schematic geology section of the study area showing the location of boreholes sampled for anarobic groundwater nanoparticles

Figure 2 shows a simplified geological cross section of the study site with the location of the boreholes used as part of this study (A-A' see Figure 1). The regional groundwater flow is along the line of section, from A' to A (Figure 2), from the made ground/landfill site to the west of Oxford towards the River Thames, see groundwater level contours in Figure 2. The connectivity

between the Terrace Gravels and the Thames is not well understood at present. The underlying Oxford Clay provides a seal at the base of the gravels. A variable thickness of alluvial silty clay (alluvium) underlies the floodplain with an alluvial silty clay soil developed at the ground surface. River gravel up to thicknesses >5 m in the middle parts of the floodplain (thinning at the margins) underlies the alluvial clay (Newell 2007). The floodplain water table is shallow and has an overlying alluvial clay cover of variable thickness and permeability, much of the underlying alluvial aquifer beneath the meadows can be considered as semi-confined throughout the year (Macdonald et al., 2007). For a more detailed description of the morphology and geology of the area see Newell (2007).

2.1 BOREHOLE INSTALLATION

The boreholes were installed in October 2010 using a Dando Terrier 2002 (Plate 1), the boreholes were completed using pvc (42 mmOD) casing with 1 mm slots in the screen. A natural pack (1-2 mm washed sand) was used around the borehole to within 500 mm of the surface, with a bentonite seal at the top of the borehole to ensure no bypass flow from the surface (Plate 2). The boreholes were completed below ground level and finished within a 100 mm drainage pipe (5-200 mm below ground level), see Plate 2. Each borehole was competed with a threaded pvc cap and covered with a metal plate for ease of locating the borehole using a metal detector. Plate 3 shows an example of a completed borehole with a threaded extension being added to the top of the borehole. Plate 4 shows a borehole with a pvc extension fitted for sampling during flooded ground conditions.

Plates 2-4 Borehole installation: 1) Drilling with a Dando Terrier 2000, 2) Borehole completion, 3) Accessing the borehole an adding extension, 4) Borehole fitted with extension for flooding

2.2 ACCESSING BOREHOLES DURING DRY AND FLOODED GROUND CONDITIONS

Each borehole was located using a GPS and a metal detector (Plate 5) during dry and flooded conditions. To sample for groundwater during flooded ground conditions it was necessary to bund the borehole using a 300 mm diameter pvc pipe and remove the surrounding flood water using a suction pump. When the surrounding flood water had been removed the extension was added to the top of the borehole taking great care to make sure that no contamination was introduced to the borehole during this stage (see Plate 6). The borehole could then be dipped to measure the water level and the Teflon inflow tube from the peristaltic pump lowered into the base of the borehole to sample the groundwater (Plate 7 and 8).

Plates 5-8 Accessing boreholes during flooded ground conditions: 5) Finding boreholes using a metal detector, 6) Accessing flooded borehole using a pvc bund and suction pump, 7) Purging a borehole prior to sampling, 8) Groundwater sampling under flooded conditons

3 Methodology

3.1 SAMPLING NANOPARTICLES IN SUB-OXIC GROUNDWATERS

The way in which a groundwater sample is collected may have a large affect the amount/type of nanoparticles and colloidal particles (defined as solid phase material with one dimension between 1 nm and 1 μm) material found in the sample (Backhus et al., 1993). For a sample to be 'representative' of the particles in suspension under natural groundwater flow it is important to not introduce colloids and nanoparticles into the groundwater system as an artefact of the sampling, or filter them out by pumping to fast relative to groundwater velocity.

Nanoparticle and colloids can be introduced as a result of the borehole construction process (e.g. drilling mud), from surface contamination during sampling, and high flow rates during pumping may shear otherwise immobile particles from localised aquifer sediments (Ryan and Gschwend 1990). This depends to some extent on the maturity and design of the borehole. A borehole that is well developed and has been in operation for some time will not be necessarily prone to the same problems of artificially induced colloidal material during pumping, as the most easily accessible material induced by construction would already have been removed from the capture zone of the borehole.

Nanoparticles may also be generated in situ due to changes in redox conditions (Ryan and Gschwend, 1994a; 1994b). The geochemistry of the groundwater system needs to be maintained, this is especially important when sampling groundwaters with anaerobic and reducing conditions. Ryan and Gschwend (1990) recommended that groundwater needs to be pumped at a low flow rate (~100 mL/min). As in the case of any representative groundwater sample the borehole needs to be purged sufficiently to remove the standing water in the borehole prior to sample collection.

Plates 9-12. Anaerobic groundwater nanoparticle sampling: 9) Filling anaerobic chamber prior to sampling, 10) Filtering samples under anaerobic conditions at nest 26, 11) Filtering samples under anaerobic conditions at nest 28, 12) Sampling under flooded conditions at nest 28

Two multi-level borehole sites, nests 26 and 28, were sampled for anaerobic groundwater nanoparticles. A pilot sampling round was carried out at both nests (28c, 28d and 26c) in December 8th 2010 to test the sampling protocol and assess the stability of the samples prior to characterisation by AFM. At both nests groundwaters from the floodplain terrace gravels were

sampled from boreholes completed at 1.5 m (samples 26c and 28c) and 3.5 (samples 26d and 28d) below ground level. The two nests were sampled on two occasions on the 24th February 2011 and on the 13th April 2011. Plates 9 to 12 show nanoparticle sampling with flooded (nest 28) and dry conditions (nest 26) in April 2011.

A protocol for sampling anaerobic groundwater nanoparticles was developed as part of this study, this is detailed below:

1. Steps were taken to eliminate the possibility of introducing surface particles to the borehole and contaminating the sample. A new, clean piece of Teflon tubing was used at each site to minimise cross contamination.
2. The boreholes were pumped using a peristaltic pump operated at a low flow rate (50-100 mL/min) to avoid particle detachment and straining during pumping.
3. The boreholes were purged by removing at least 3 borehole volumes prior to sampling and nanoparticle sampling was only carried out when stable field chemistry measurements (dissolved oxygen (DO), redox potential (Eh), conductivity (SEC) and pH) were obtained in a sealed flow-through cell. An Aquameter ^{TM} (Watterra) multi parameter probe was used to monitor these field parameters (see plates 7 and 8).
4. Sampling was carried out in a portable anaerobic chamber filled with nitrogen gas (oxygen free grade, BOC). The chamber was filled with nitrogen gas in advance of the sampling and the atmospheric dissolved oxygen monitored (portable Metler-Toledo meter) during the sampling to ensure that anaerobic conditions were maintained throughout (see plate 9).
5. Groundwater pH was monitored to ensure that CO_2 degassing was not significantly changing the chemistry of the groundwater as a result of the anaerobic nitrogen chamber.
6. Groundwater samples were filtered using 0.1 μm Whatman filters to remove particles >0.1 mm. The filters were washed with $NaNO_3$ and rinsed with ultrapure water to minimise Ca bridging on the membrane surface during filtration. Two filters were used for each sample to minimise clogging of the surface membrane and exclusion of nanoparticles.
7. Samples were pre-filtered into acid washed HDPE bottles and filled to the top to minimise the gas space at the top of the bottle and capped securely. Duplicate samples were taken on each occasion (see Plates 10 and 11).
8. Samples were then placed in an air tight container (see Plate 10), surrounded by an outer jacket of groundwater (as per methods for CFC and SF_6 dissolved gas sampling for groundwater dating techniques, see Busenberg and Plummer (1992)) to exclude any possibility atmospheric contamination during transportation prior to analysis.
9. Once sealed the sample could then be removed from the anaerobic chamber for transportation to the FENAC laboratory in a cool box.

When the field parameters (DO, Eh, pH, SEC) were stable and the boreholes had been purged sufficiently groundwater samples from each borehole were taken for analysis for major and minor inorganic chemistry, dissolved organic carbon (NPOC) and dissolved fluorescent organic matter (FOM). This was done prior to the nanoparticle sampling. Samples for inorganic analysis were filtered using 0.45 μm Whatman ^{TM}, cellulose nitrate filters and stored in sterile Nalgene containers. Samples for dissolved organic carbon and fluorescence analysis were filtered using silver nitrate filters and stored in glass containers. Cations were preserved by acidification with 1% v/v nitric acid (Aristar). Bicarbonate concentrations were determined by titration in the field.

3.2 GROUNDWATER CHEMISTRY

Cations were analysed by ICP-MS, anions by HPLC, NPOC using a CO_2 analyser following acidification and sparging. A Varian^{TM} Cary Eclipse fluorescence spectrometer was used for the

fluorescent organic matter (FOM) analysis. Excitation (Ex) wavelengths were set between 200 and 400 nm with a 5 nm bandwidth and emission (Em) wavelengths were set between 250 and 500 nm with a 2 nm bandwidth, see Lapworth et al (2008) for details on fulvic-like (FA-like) analysis.

3.3 CHARACTERISING NANOPARTICLES IN SUB-OXIC GROUNDWATERS

Nanoparticle characterisation was carried out using a number of state-of-the-art techniques that are available at FENAC. AFM, TEM and ESEM techniques were used to characterise the particle size distribution of nanoparticles in the anaerobic groundwaters (e.g. Balnois et al., 1999, Winkinson et al., 1999, Lead et al., 1999). AFM measures the nanoparticle topography/height of the nanoparticles on a mica surface on the basis of the repulsion or attractive forces between sample and the AFM tip. ESEM is an imaging technique that is able to quantify the size and morphology of the nanoparticles, and has been used to calculate fractal dimensions of humic substances (Redwood et al., 2005). ESEM coupled to energy dispersive x-ray (SEM-EDX) analysis was used to carry out particle size determination and elemental analysis of the nanoparticles. FFF coupled to a fluorescence detector was used to investigate the dissolved organic matter characteristics and diffusion coefficients of nanoparticles in our samples (Baalousha et al., 2006, Baalousha and Lead, 2007). FFF is an important separation technique based on hydrodynamic principles in which particles are separated based on their interaction with a crossflow field force and their translational diffusion.

These methods were modified to retain the integrity of the sample nanoparticle distribution during sample preparation and analysis. AFM and TEM analysis was carried out in anaerobic chamber filled with oxygen free nitrogen gas (BOC). FFF analysis was carried using mobile phases that were free from dissolved oxygen, i.e. purged with nitrogen gas, to stop the in-situ formation of nanoparticles during analysis.

Once a sampling and storage method had been tested in the December round, and found to be satisfactory for AFM, the methodology was extended to other characterisation techniques. In subsequent rounds all four samples were analysed by AFM, samples were analysed by TEM from the February round and samples were taken for FFF in the April round.

3.3.1 Atomic force microscopy (AFM)

All sample preparation and analysis with AFM were carried out within 36 hours after the groundwater sampling. The groundwaters (sub-oxic and aerated aliquots) were transferred to 5 mL vials under nitrogen atmosphere, and sheets of freshly cleaved mica (Agar Scientific) were inserted vertically into the samples for 30 min, letting particles from the sample adhere to the mica. The mica sheets were thereafter rinsed by immersing in sub-oxic (nitrogen bubbled) ultrapure water for a few seconds, followed drying under 100 % humidity in nitrogen atmosphere for a few hours. With the AFM-instrument (Park System XE-100) placed in a laminar glove box with nitrogen-atmosphere, AFM-images were acquired over different areas (0.5×0.5 µm, 1×1 µm, 2×2 µm, 5×5 µm, 20×20 µm etc.) of the mica, in non-contact mode using a silicon cantilever with 42 N m^{-1} force constant and 330 kHz frequency. For each sample, the size distribution of 210 particles was determined by measuring the maximum height above the mica of 25-35 particles on at least 6 different 2×2images.

3.3.2 Transmission and scanning electron microscopy (TEM and SEM)

Samples for TEM and SEM were prepared under nitrogen atmosphere, by placing droplets of the samples (sub-oxic and aerated aliquots) on Forvar/carbon coated 300 mesh Cu TEM grids placed horizontally on a clean surface. After 30 min, the grids were rinsed by immersing in sub-oxic (nitrogen bubbled) ultrapure water for a few seconds, followed by drying under nitrogen atmosphere. Within a couple of weeks, TEM (JEOL 1200EX) images were acquired at 80 keV,

on five different areas of the grids, each area at 30 000, 100 000, 300 000 and 500 000 times magnification. The SEM-instrument (JEOL 7000) was equipped with a scanning TEM (STEM) unit and energy-dispersive X-ray diffraction (EDX) for element analysis. On different areas of the grids, images were acquired by both SEM and STEM with secondary electrons (SEI) and backscattered electrons (BSE), and the major element composition was determined by EDX on four different particles and on the background grid.

3.3.3 Field-flow Fractionation (FFF)

The asymmetrical FFF instrument (AF 2000, Postnova Analytics) had a channel defined by a 0.35 mm spacer and a 1 kDa nominal cut-off ultrafiltration membrane of regenerated cellulose (Postonva Analytics). The FFF-carrier solution, made up of 10 mM NaCl with pH 8, was made sub-oxic by continuous bubbling with nitrogen. 10 mL of the groundwater samples (sub-oxic and aerated aliquots) were injected and focused in the channel with a tip flow of 0.5 mL min^{-1} and a focus flow of 2.5 mL min^{-1} for 30 min, followed by elution and fractionation with a crossflow of 3 mL min^{-1} and detector flow of 0.5 mL min^{-1}. Nanoparticles eluting from the FFF-channel were detected on-line with UV-absorbance at 254, 350, 400, 575 and 700 nm, fluorescence at excitation/emission 350/450 nm and multi-angle light scattering at 35°, 50°, 75°, 90°, 105°, 130° and 145°. The continuous size distributions of nanoparticles were determined by converting retention time into diffusion coefficient and equivalent hydrodynamic diameter using the FFF-theory, after calibrating the FFF channel thickness using two proteins (bovine serum albumin and ferritin) with known diffusion coefficients.

3.4 NANOPARTICLE CHARACTERISATION FOLLOWING AERATION

The groundwater nanoparticles were also characterised following aeration by bubbling air through the sample. This was carried out under controlled laboratory conditions to investigate the evolution of nanoparticles. In the anaerobic groundwaters where Fe is dissolved as Fe(II) this will be oxidised via Fe(III) to Fe(hydr)oxides (Liang et al., 1993).

4 Results and discussion

4.1 GROUNDWATER CHEMISTRY

Table 1 details the field chemistry and dissolved (<0.45 μm) and particulate (>0.45 μm) groundwater chemistry for each site during the December sampling round. Groundwater chemistry for selected redox sensitive parameters (DO, Eh, Fe) and landfill plume tracers (e.g. NPOC and HCO_3) are shown in Table 2 for all three nanoparticle sampling rounds. The dissolved oxygen concentrations at each site were less than 0.5 mg/L. The high dissolved Fe and Mn suggest that the groundwaters are Mn and Fe reducing, it is also possible that the Fe and Mn could have migrated from an up-gradient source (see Christensen et al., 2000). The absence of nitrate is a clear indication that nitrate reduction is occurring in these shallow anaerobic groundwaters. High NH_4 and low NO_3 concentrations indicate that dissimilatory nitrate reduction to ammonium may be important. Redox potential (Eh) for samples from nest 26 were found to be slightly more reducing (ca.+150 mV) than those from nest 28 (ca. +200 mV). All the samples have comparable pH values of around 6.8. Arsenic concentrations in nest 26 are significantly higher than in nest 28, and exceed the WHO drinking water limit of 10 ug l^{-1}. This could be due to reductive dissolution of iron (III) oxy-hydroxides and this is supported by the consistently higher Fe concentrations in nest 26. Colloidal and nano-scale clay and Fe particles could be important vectors for NH_4 and As migration within the landfill plume due to their high surface area and potential for rapid transport within the shallow aquifer.

Table 1 Groundwater chemistry

Parameter	Unit	26c	26d	28c	28d
Ca	mg l^{-1}	259	229	202	173
Mg	mg l^{-1}	34.0	49.4	48.3	40.9
Na	mg l^{-1}	75.7	83.3	94.2	87.7
K	mg l^{-1}	23.6	40.2	51.2	52.9
Si	mg l^{-1}	6.45	7.75	6.7	7.4
HCO_3^-	mg l^{-1}	858	880	980	1009
Cl^-	mg l^{-1}	72.3	84.1	88.3	81.7
SO_4^{2-}	mg l^{-1}	228	253	160	127
NO_3^-	mg l^{-1}	0.079	0.040	0.031	0.043
NPOC	mg l^{-1}	8.5	10	7.0	8.9
FA-like FOM	RU	3.1	3.0	3.1	3.7
Si*	mg l^{-1}	6.45	7.75	6.71	7.43(10)
Ba	µg l^{-1}	86.4	52.0	73.5	71.1
Sr*	µg l^{-1}	650	646	931	1074(7)
Mn*	µg l^{-1}	2102	3008	1749(7)	2252
Total Fe*	µg l^{-1}	9419	9669	1438(7)	1273
Al	µg l^{-1}	3	3	5	2
U	µg l^{-1}	0.29	0.87	3.32	2.09
As	µg l^{-1}	14.1	11.4	4.5	4.9
SRP	µg l^{-1}	11	7	65	5
NH_4^+	mg l^{-1}	15	23	43	51

* % particulate (>0.45 µm) shown in parenthesis, RU=Raman units, results from 8th December sampling for all parameters except NH_4 and SRP (soluble reactive P) which is an average of results from sampling in February and April.

There is some evidence of particulate Si and Sr at site 28d, and particulate Mn and Fe at site 28c (Table 1). All the groundwaters have fairly high SEC (c. 2000 µS cm^{-1}), and can be characterised as Ca-HCO_3 type waters. The reason for the high total dissolved solids is due to the proximity of the boreholes to a landfill site and the presence of a contaminant plume down gradient of this source.

Table 2 Chemistry for selected redox parameters and landfill contaminant tracers during the three nanoparticle sampling rounds

Sample	Field Eh mV	Field pH	Field HCO_3^- mg L^{-1}	Field DO_2 mg L^{-1}	NPOC mg L^{-1}	Total Fe mg L^{-1}
8th December 2010						
26c	147	6.84	858	0	8.5	9.4
26d	154	6.85	880	0	10	9.7
28c	203	6.83	980	0	7	1.4
28d	207	6.84	1009	0.3	8.9	1.3
24th February 2011						
26c	147	6.8	672	0	8.2	10
26d	142	6.75	750	0	8.0	10.5
28c	167	6.74	836	0	7.8	2.3
28d	169	6.85	890	0.24	9.8	1.7
13th April 2011						
26c	159	6.8	812	0.9	9.8	10.5
26d	149	6.85	859	1.1	7.7	9.9
28c	108	6.86	985	0.9	8.3	3.5
28d	177	6.84	1000	1.1	7.9	1.6

4.2 NANOPARTICLE CHARACTERISATION

4.2.1 Atomic force microscopy

Figure 4 shows the distribution of AFM particle heights for the three sites sampled in December as part of the pilot study. Summary statistics for AFM data from the December round are shown in Table 3. For the AFM data a Kruskal-Wallis test was carried out on the three samples to investigate whether the population distributions are identical without assuming them to follow the normal distribution. This test returned a *p*-value of <2.2e-16. It is therefore concluded that the particle size populations are nonidentical for the three samples at the 1e-15 significance level. The cumulative frequency plot suggests that there are at least two populations for the nanoparticles characterised by AFM.

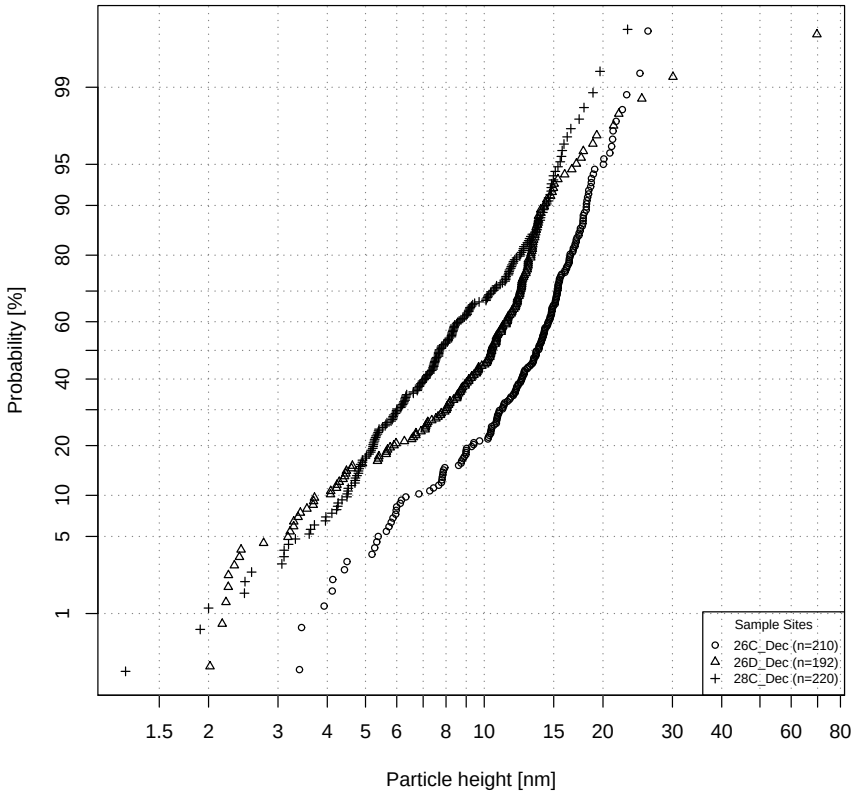

Figure 3 Cumulative probability plot for particle height by AFM for sites 26c (n: 210), 26d (n: 192) and 28c (n: 220) from 8th December 2010

Table 3 Summary statistics for particle height from AFM analysis of pilot sampling round on 8th December 2010

Statistic (nm)	26c	26d	28c
Min	3.4	2	1.2
25th Percentile	10.5	7.1	5.6
Median	13.6	10.4	7.7
Mean	13.1	10.3	8.6
75th Percentile	15.7	12.6	11.5
Max	26	69.7	23.1

Table 4 Average particle sizes determined by AFM for samples taken in 8th December 2010 and 24th February 2011

Sample	December	February
26c	13.1 ± 4.3	9 ± 4.2
26d	10.3 ±6.1	11 ±7.1
28c	8.6 ± 3.9	11 ± 3.9
28d	N/A	9 ± 9.8

Average particle sizes,± 1 x standard deviation, determined by AFM for samples taken in the December and February rounds are shown in Table 4,. Selected 2×2 µm AFM-images and histogram with particle size distributions are shown in Figures. 4-11. Additional AFM-images are available. Field measurements of Eh indicated slightly more reducing conditions in samples

26c and 26d than in 28c and 28d, while dissolved oxygen (DO_2) was below detection limit in all samples except for 28d, which had a slightly higher DO_2 of 0.24 mg L^{-1}. Sample 28d was also slightly higher in dissolved organic carbon (NPOC, 9.8 mg L^{-1}) than the other samples (7.8-8.2 mg L^{-1}). The biggest difference in chemistry between the samples was for dissolved iron, which was much higher in the 26c and 26d samples (10.0-10.5 mg L^{-1}) than in the 28c and 28d samples (1.7-2.3 mg L^{-1}). The AFM-images of all the sub-oxic groundwater samples were dominated by nearly spherical nanoparticles, with a size distribution mostly in the 1-20 nm range, centred at around 10 nm (Figures. 4, 6, 8 and 10).

The average particle size was not significantly different between the different samples, but some variations could be observed between images. In the sub-oxic sample 26c, images A1 and B1 (Figure. 4) contained almost exclusively nanoparticles smaller than 10 nm (Figure. 4, A2 and B2), while the nanoparticles on the other images (Figure. 4, C1, B1, E1, F1) were largely >10 nm (Figure. 4, C2, D2, E2, F2). In the sub-oxic sample 26d (Figure. 6), the images C1, E1 and F1 appeared to have bi-modal particle size distributions, with larger (up to 40 nm) nanoparticles in addition to the main population around 10 nm.

Similar bi-modal size distributions could be observed in sample 28c, images C2, D2, F2 (Figure 8) and 28d, images A1, B1, C, E1 and F1 (Figure. 10). Sample 28d had the broadest particle size distribution (Table 4), with large amounts of very small (around 5 nm) nanopaticles and larger nanoparticles distributed up to 55 nm (Figure. 10G). It is possible that the broader size distribution of sample 28d was a result of the higher concentration of dissolved oxygen in that sample, resulting in increased oxidation and growth of iron-rich nanoparticles.

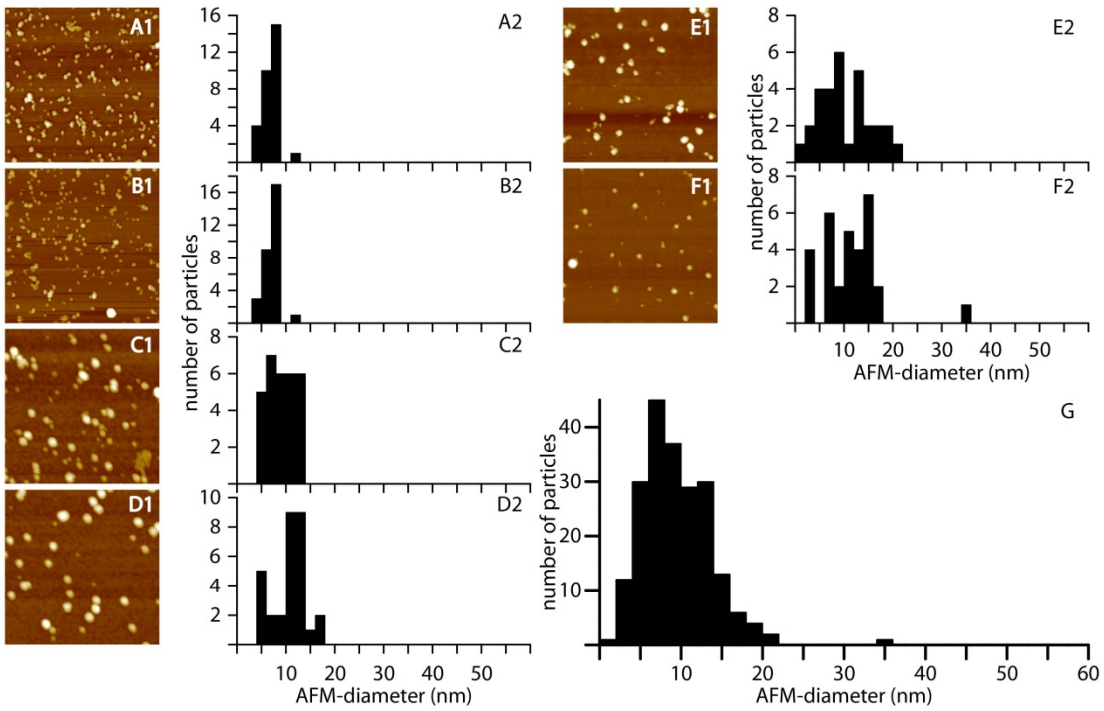

Figure 4 Sample 26c from February 24th under sub-oxic conditions; selected 2×2 µm AFM-images (A1-F1), particle diameter distributions (n: 25-35) on the discrete images (A2-F2) and cumulative particle size distribution (n: 210) of all images (G).

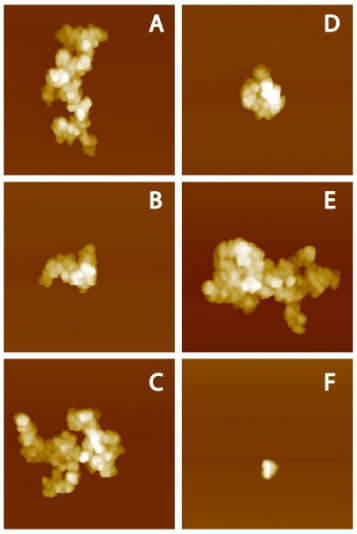

Figure 5 Sample 26c from February 24th after aeration; selected 2×2 µm AFM-images (A-F).

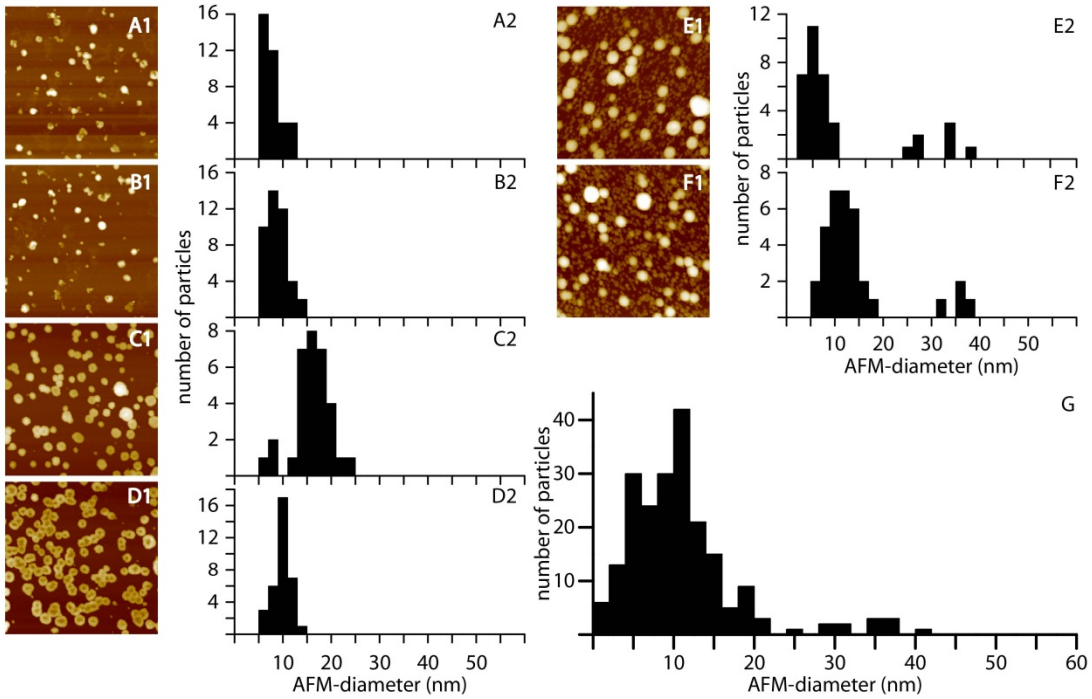

Figure 6 Sample 26d from February 24th under sub-oxic conditions; selected 2×2 µm AFM-images (A1-F1), particle diameter distributions (n: 25-35) on the discrete images (A2-F2) and cumulative particle size distribution (n: 210) of all images (G).

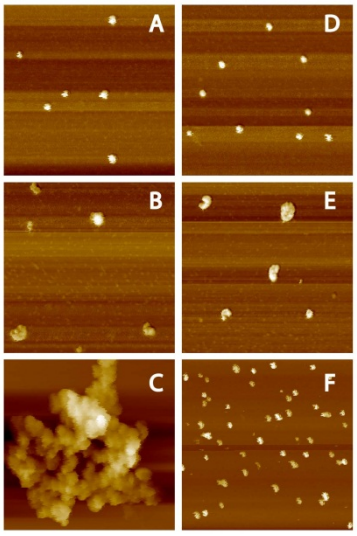

Figure 7 Sample 26d from February 24th after aeration; selected 2×2 µm AFM-images (A-F).

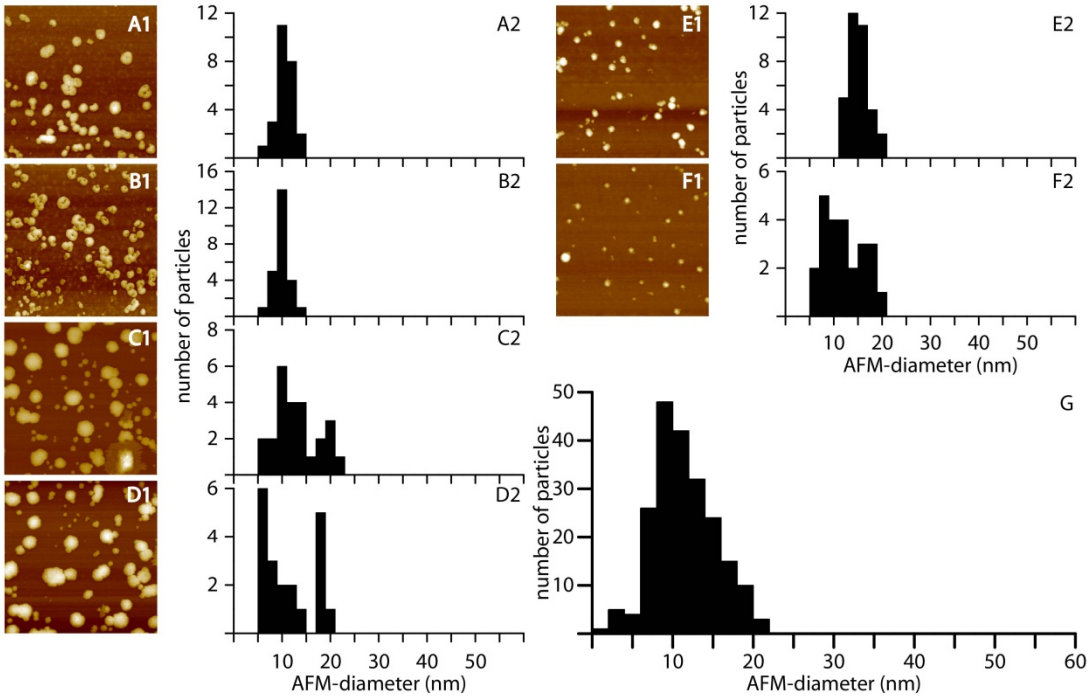

Figure 8 Sample 28c from February 24th under sub-oxic conditions; selected 2×2 µm AFM-images (A1-F1), particle diameter distributions (n: 25-35) on the discrete images (A2-F2) and cumulative particle size distribution (n: 210) of all images (G).

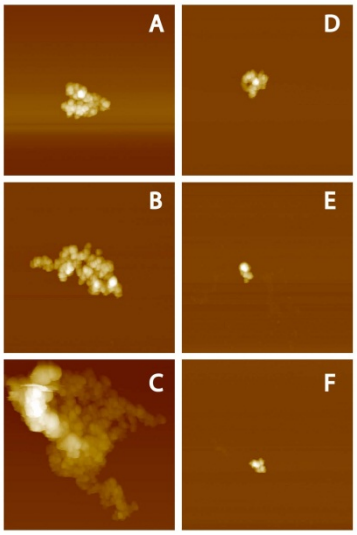

Figure 9 Sample 28c from February 24th after aeration; selected 2×2 µm AFM-images (A-F).

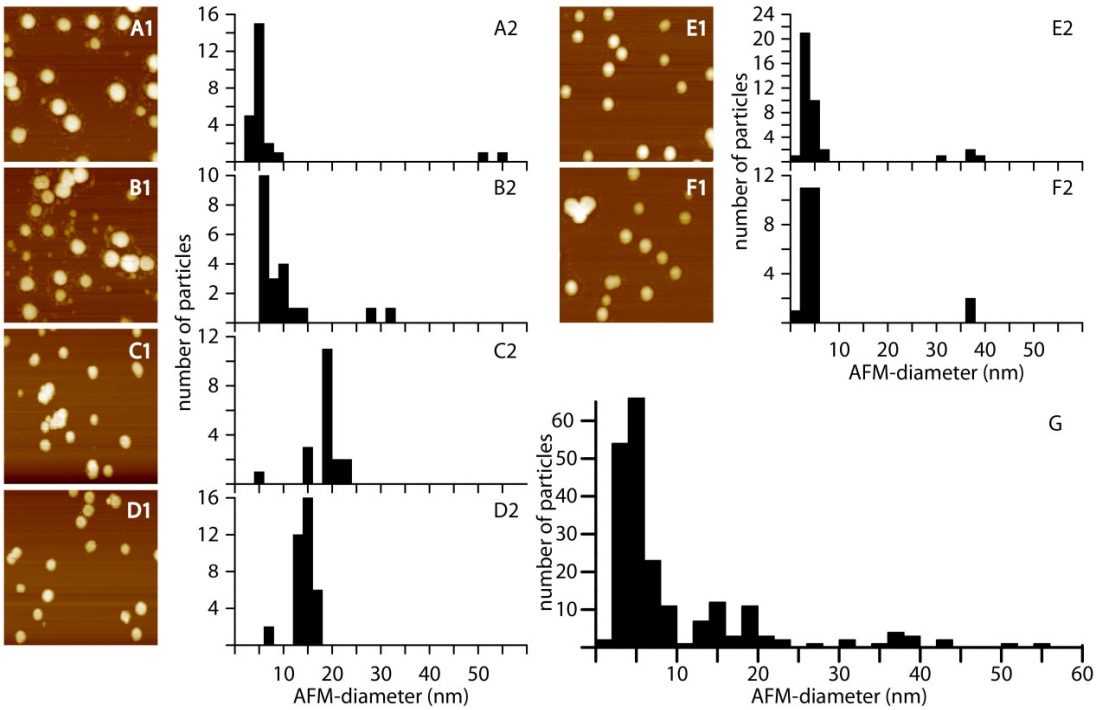

Figure 10 Sample 28d from February 24th under sub-oxic conditions; selected 2×2 µm AFM-images (A1-F1), particle diameter distributions (n: 25-35) on the discrete images (A2-F2) and cumulative particle size distribution (n: 210) of all images (G).

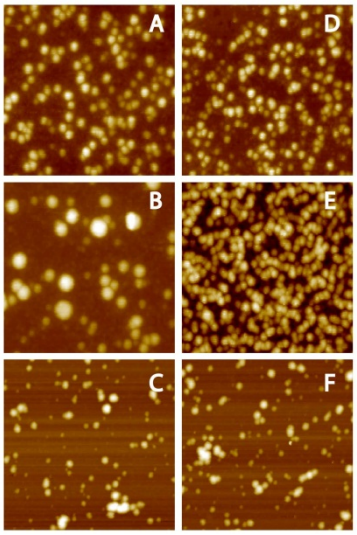

Figure 11 Sample 28d from February 24th after aeration; selected 2×2 µm AFM-images (A-F).

The deeper sites (26d and 28d) had higher frequencies of larger nanoparticles (30-50 nm) for both sampling rounds compared with the shallow sites. Aeration of the samples often changed the particle size distribution dramatically. For example, in the aerated sample 26c, no nanoparticles could be found on by AFM. Instead, a few large (> 100 nm) colloids were observed, that appeared to be composed of smaller nanoparticles (Figure. 5). Similar observations were made in the aerated samples 26d (Figure. 7) and 28c (Figure. 9), although nanoparticles could still be observed by AFM in sample 26d. The observations are likely to be explained by the oxidation of iron in the samples, and increased formation of iron oxyhydroxide, giving rise to aggregation of the nanoparticles. In sample 28d, large amounts of nanoparticles were observed also after aeration of the sample (Figure. 11). The fact that aggregation appeared to be less prominent in the 28d sample could possibly be explained by the much lower dissolved Fe/NPOC ratio in 28d (0.18) compared with 26c (1.2), 26d (1.3) and 28c (0.3), resulting in a higher stability of the nanoparticles in the 28d sample.

4.2.2 Transmission electron microscopy

The TEM-results should be treated by some caution, since the TEM-grids were stored for several days-weeks before analysis. Although the grids were dried, the possible formation of iron oxyhydroxide nanoparticles and colloids due to iron oxidation during storage should be taken into consideration.

Different types of particles could be observed from the TEM-micrographs. Nanoparticles of a few nm in size were observed in the sub-oxic samples 26c (Figure. 12) and 28c (Figure. 16), but never in the aerated samples, i.e., the same observation that was made from the AFM-images. Larger colloids with darker shade (i.e., less transparent for electrons) were observed in all samples, and had similar shapes as the colloids observed by AFM in the aerated samples. It is likely that these ‘dark’ colloids are iron-rich, e.g., composed of iron oxyhyroxide. The fact that the dark colloids were observed in the sub-oxic samples by TEM but not by AFM can be explained by the fact that the probability of finding them with AFM was much lower, since AFM-images were acquired on random locations of the mica substrate, while TEM-micrographs were acquired on particles selected after searching large areas of the TEM-grids. In addition, the electron dense Fe particles show up clearly on the TEM images while less dense (e.g. organic) are harder to see.

In the aerated samples 26c (Figure. 13) and 26d (Figure. 15), the sizes of the dark colloids were considerably larger compared with the sub-oxic samples, e.g., the same observation as made by AFM. In the sub-oxic samples 28c (Figure. 17) and 28d (Figure. 19), another type of colloids was observed that were ligher in shade, i.e., more transparent to electrons. A likely constituent of

these ‘light’ colloids is organic matter. In both samples, the light colloids were partly covered by ‘dark’ material, thus it appears that the light colloids function as nuclei for the growth of the presumed iron oxyhydroxide. If this is the case, the fact that no light colloids were observed in the sub-oxic samples 26c and 26d could be explained by that they were completely covered by iron oxyhydroxide, due to the much higher iron-concentration and Fe/NPOC ratios in these samples (Table 5). The presence of dissolved Fe(II) and nanoparticulate Fe(III) suggests that NPOC from the landfill has dissolved Fe(III) oxides (reductive dissolution) and produced in situ colloidal and nanoparticulate Fe oxides (Liang et al., 1993). In the sub-oxic sample 28c (Figure. 16), fibrillar material was also observed in association with the dark colloids, presumably biopolymeric organic matter.

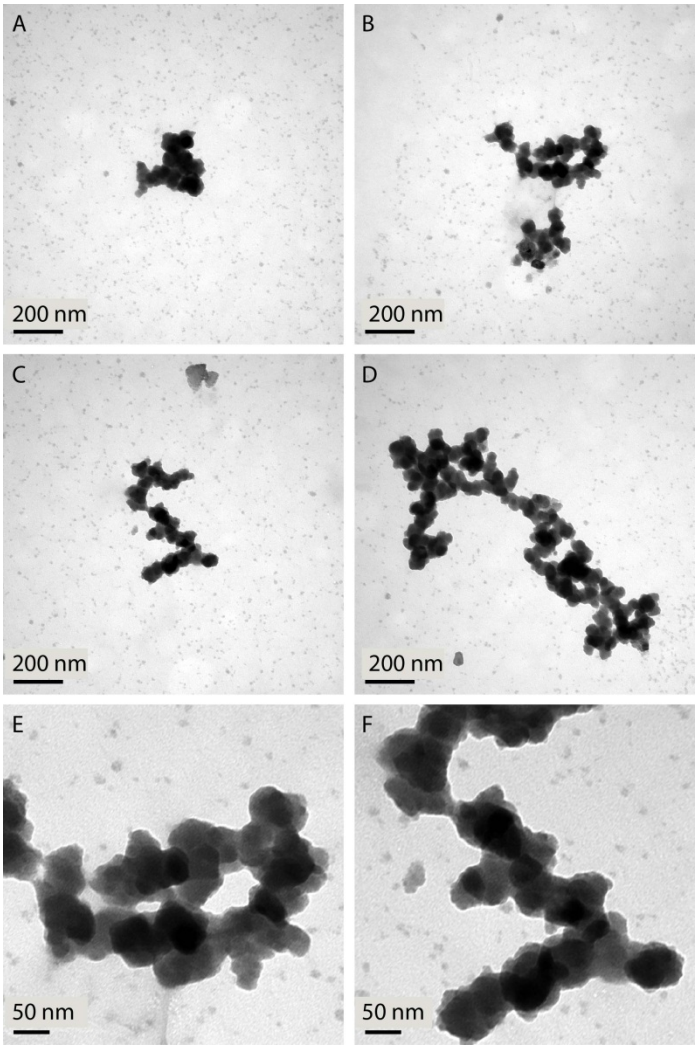

Figure 12 Sample 26c from February 24th under sub-oxic conditions; selected TEM-micrographs magnified 100 000 times (A-D) and 300 000 times (E and F).

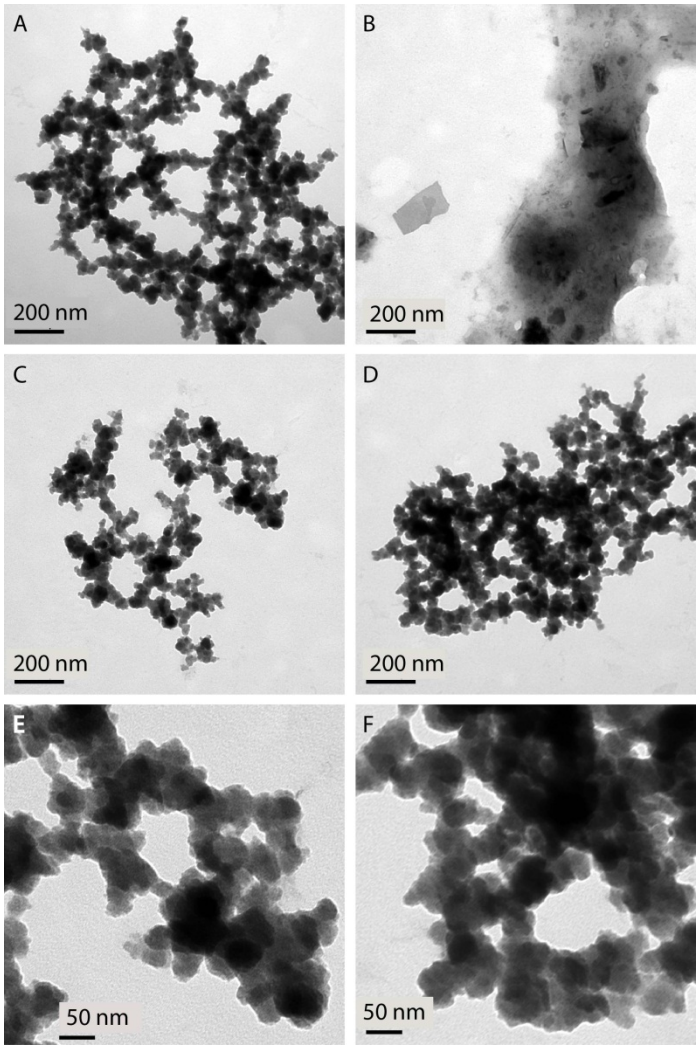

Figure 13 Sample 26c from February 24th after aeration; selected TEM- micrographs magnified 100 000 times (A-D) and 300 000 times (E and F).

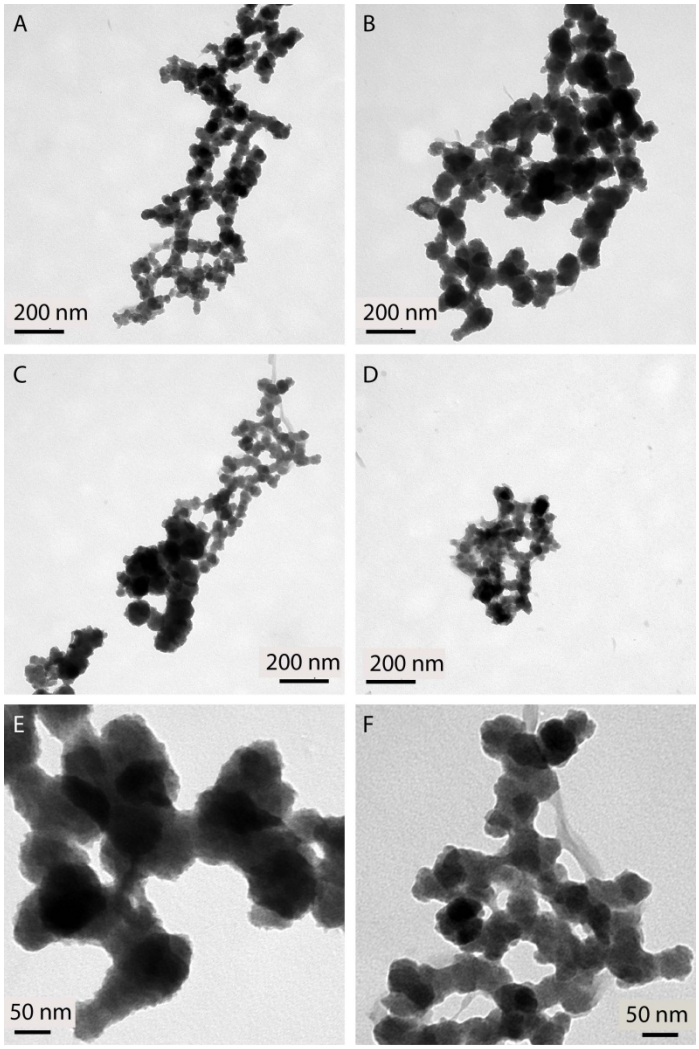

Figure 14 Sample 26d from February 24th under sub-oxic conditions; selected TEM-micrographs magnified 100 000 times (A-D) and 300 000 times (E and F).

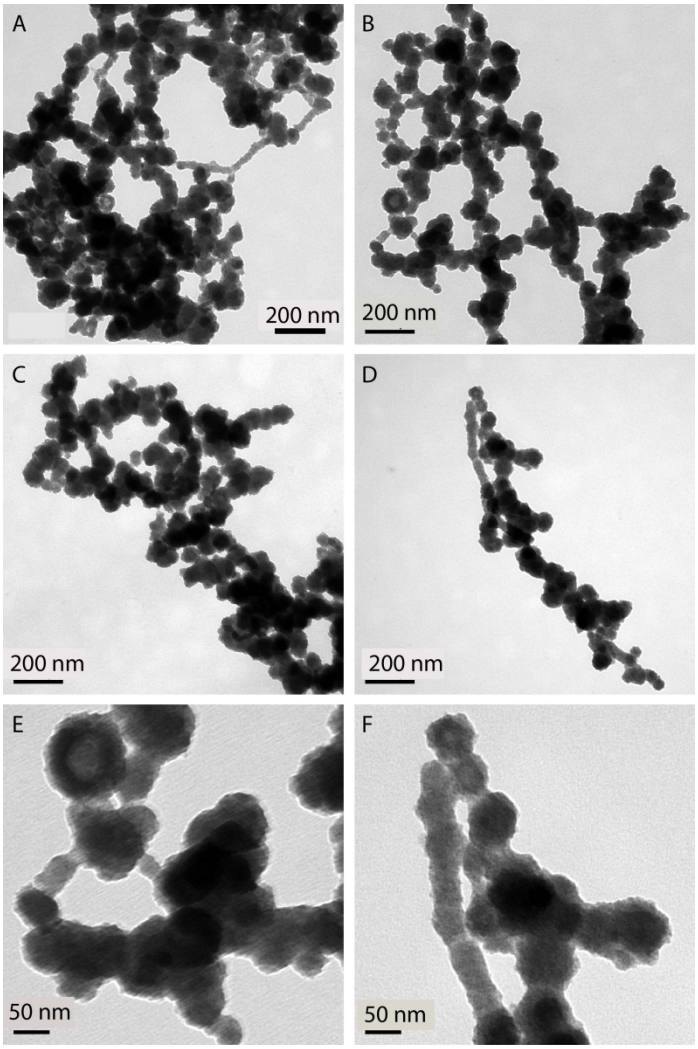

Figure 15 Sample 26d from February 24th after aeration; selected TEM- micrographs magnified 100 000 times (A-D) and 300 000 times (E and F).

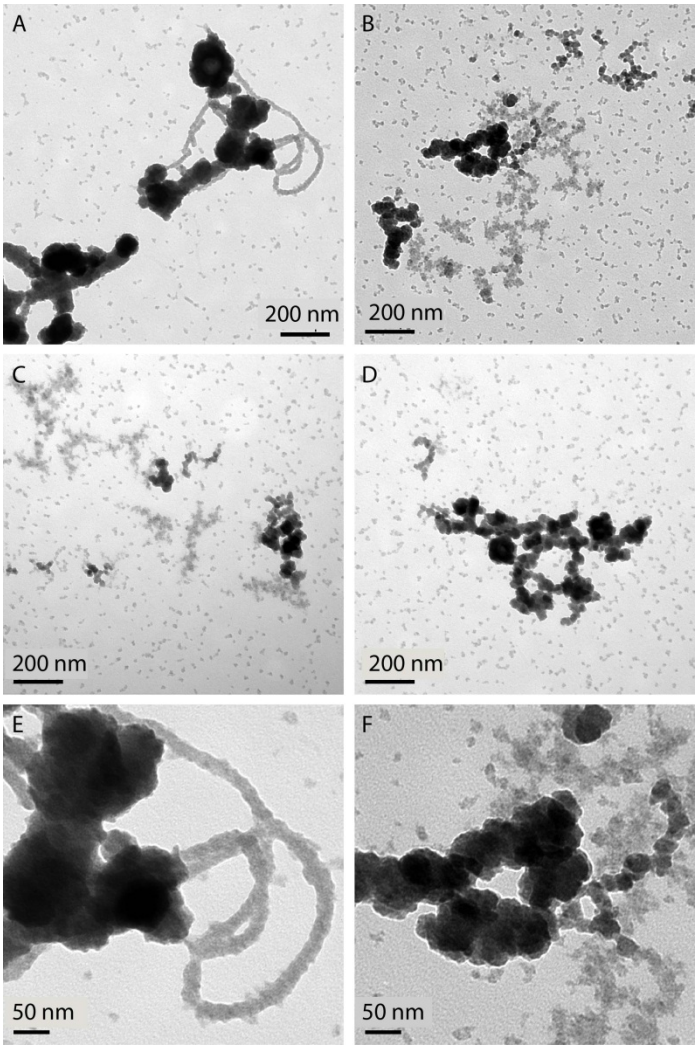

Figure 16 Sample 28c from February 24th under sub-oxic conditions; selected TEM-micrographs magnified 100 000 times (A-D) and 300 000 times (E and F).

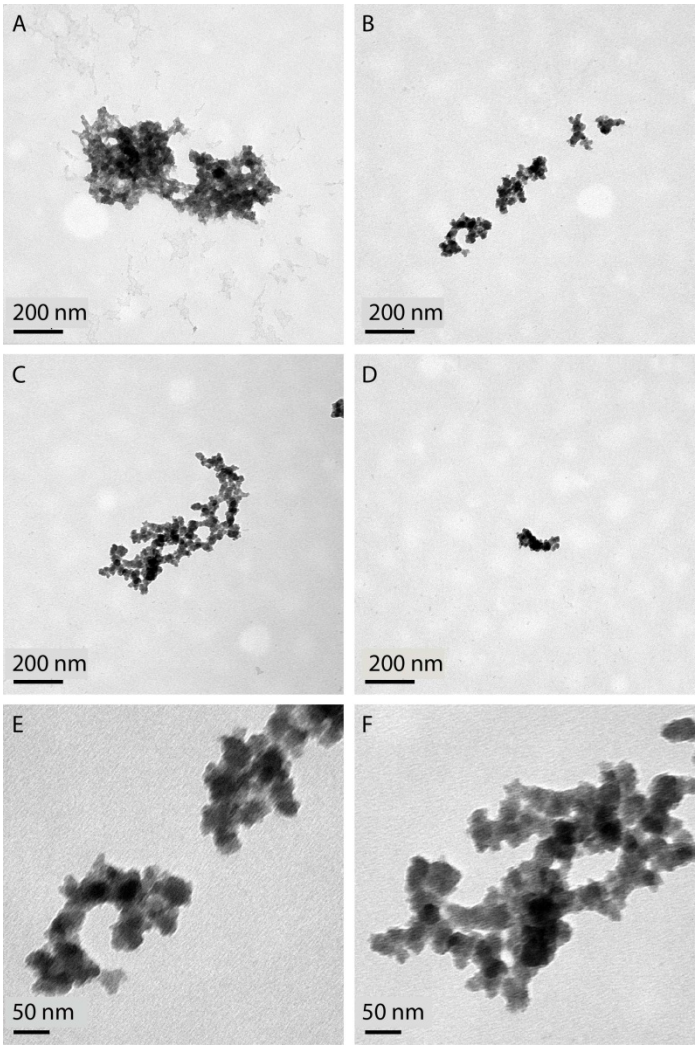

Figure 17 Sample 28c from February 24th after aeration; selected TEM- micrographs magnified 100 000 times (A-D) and 300 000 times (E and F).

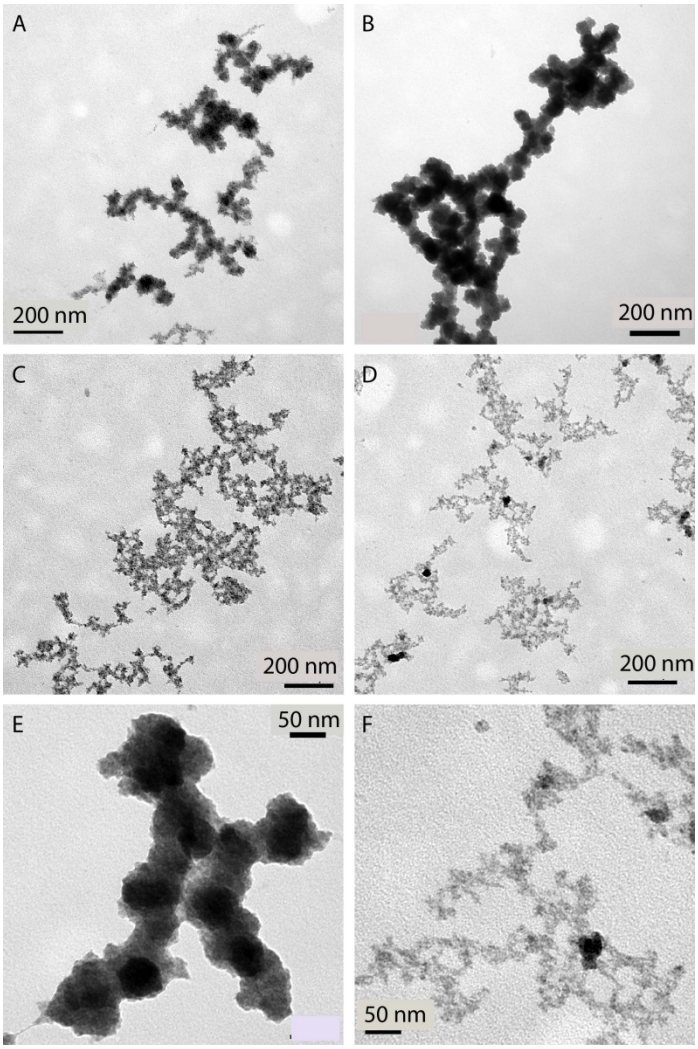

Figure 18 Sample 28d from February 24th under sub-oxic conditions; selected TEM-micrographs magnified 100 000 times (A-D) and 300 000 times (E and F).

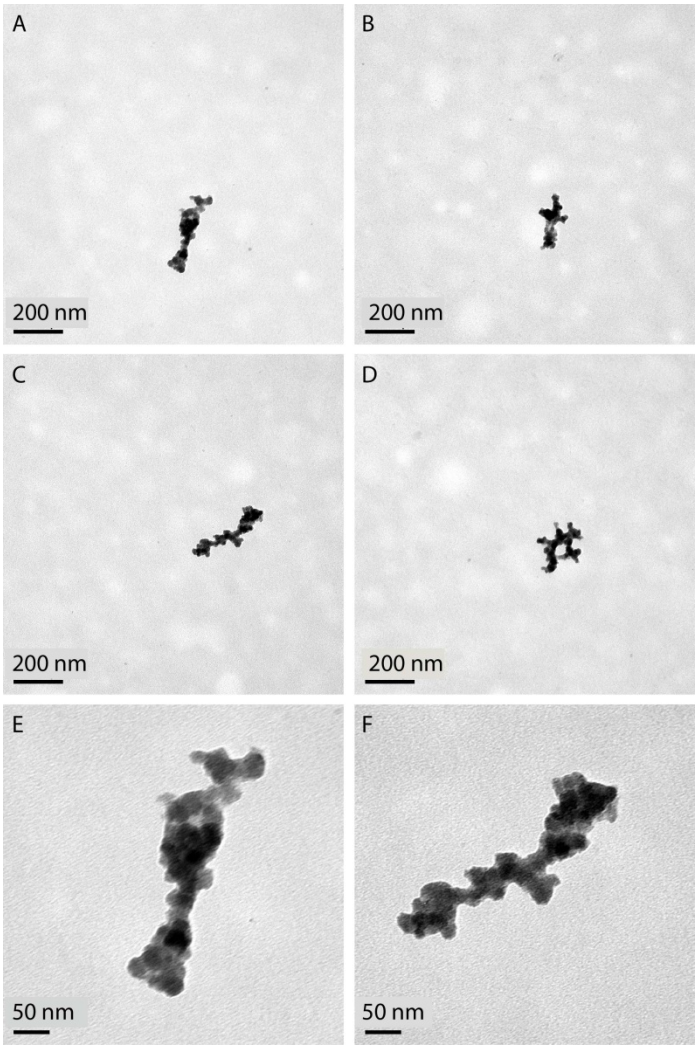

Figure 19 Sample 28d from February 24th after aeration; selected TEM-micrographs magnified 100 000 times (A-D) and 300 000 times (E and F).

4.2.3 Scanning electron microscopy with energy dispersive X-ray diffraction

The SEM-micrographs of the sub-oxic samples showed colloids with similar shapes as the dark colloids on the TEM-micrographs, and as the colloids found by AFM in the aerated samples (Figure 20-23). EDX-spectra taken on these colloids showed high Fe-signals, confirming that the colloids were iron-rich. In addition, the Ca signal was higher compared with background EDX-spectra from the TEM-grids, indicating that the colloids were rich in Ca. P peaks were present in nanoparticles enriched in Fe from samples from nest 28 (Figures 22 and 23) while they were absent in the samples from nest 26 (Figs. 20 and 21). This shows evidence of P association with Fe nanoparticles, perhaps indicating PO_4 binding to Fe oxy-hydroxides, most likely from nearby surface water sources of soluble reactive P. Compact particles (see 16(1)) were also observed, giving very high Ca-signal in EDX, suggesting that they could be composed of calcite.

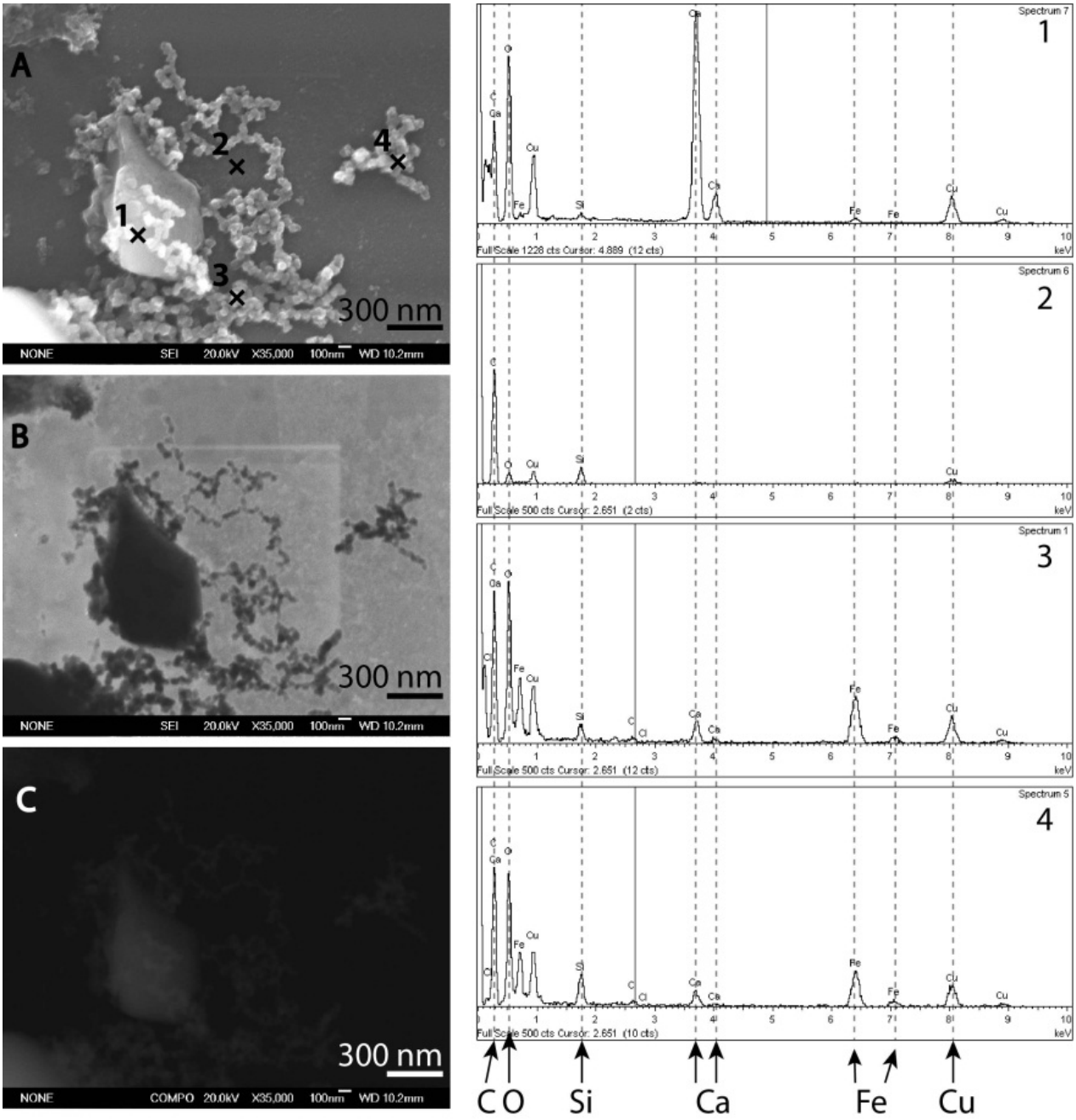

Figure 20 SEM (A), STEM images from secondary electrons (B) and backscattered electrons (C) from sample 26c under sub-oxic conditions, taken on February 24th. EDX-spectra showing major element-composition at different positions of the image (1,2,3 and 4).

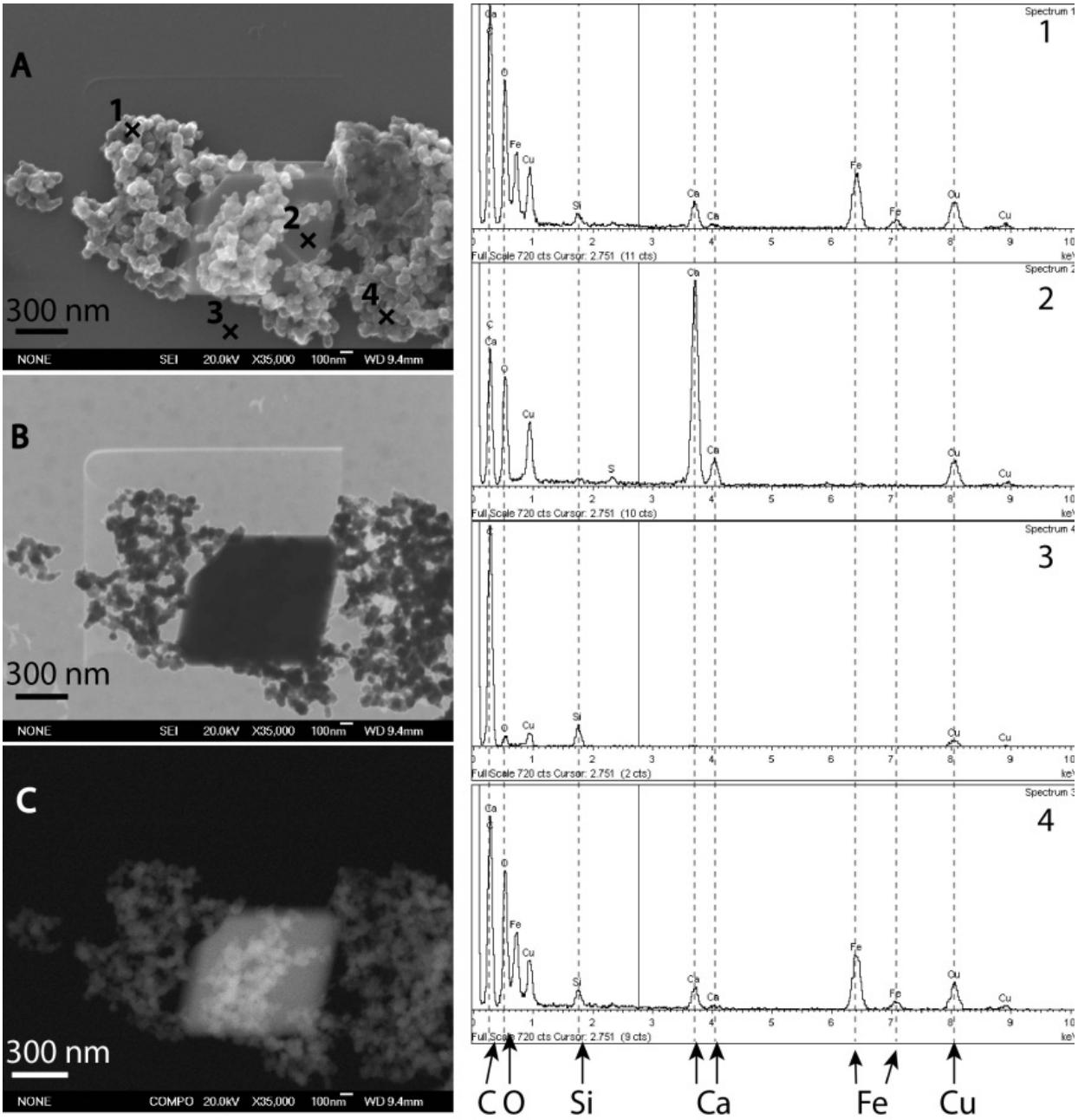

Figure 21 SEM (A), STEM images from secondary electrons (B) and backscattered electrons (C) from sample 26d under sub-oxic conditions taken on February 24th. EDX-spectra showing major element-composition at different positions of the image (1,2,3 and 4).

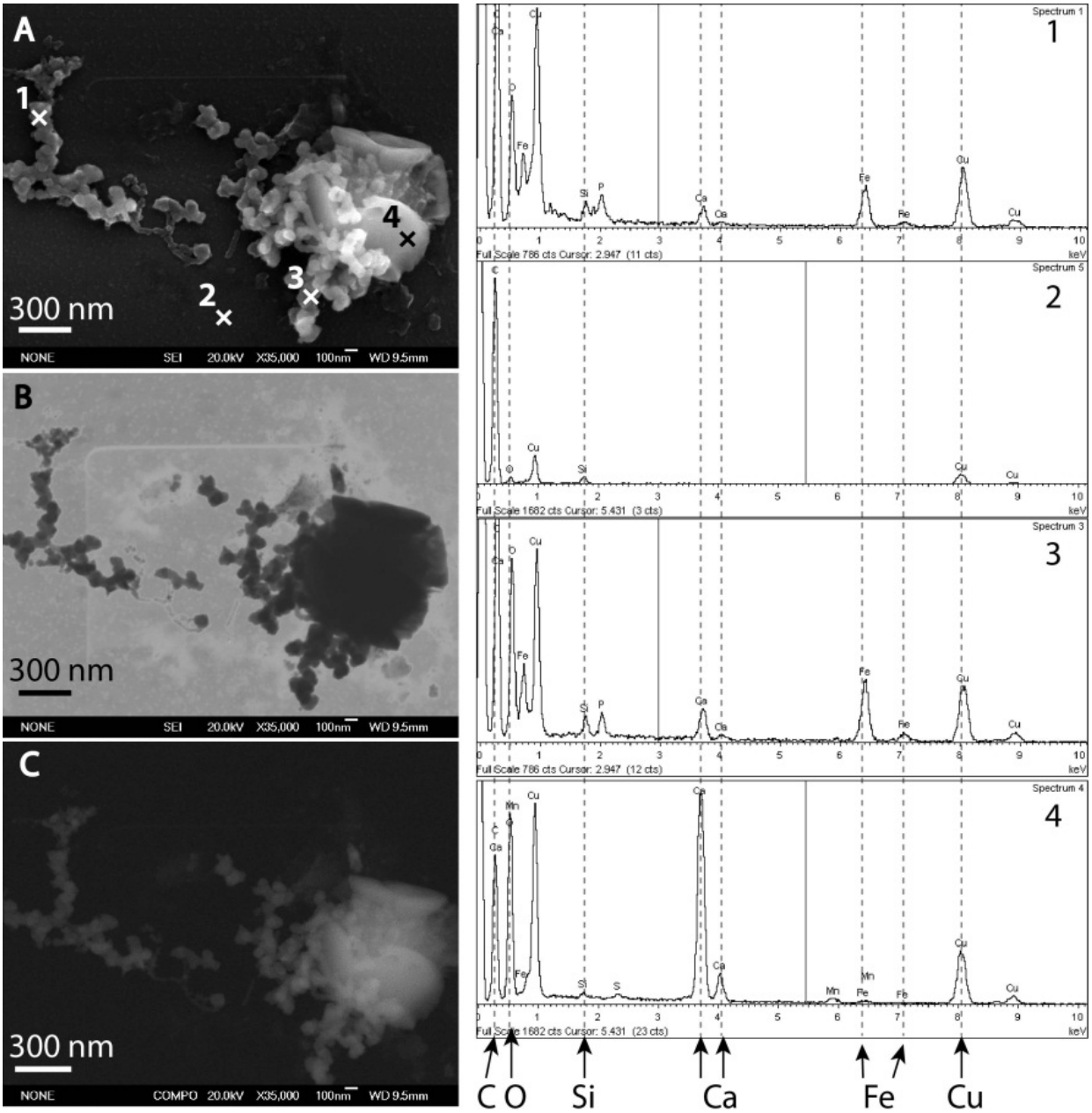

Figure 22 SEM (A), STEM images from secondary electrons (B) and backscattered electrons (C) from sample 28c under sub-oxic conditions taken on February 24th. EDX-spectra showing major element-composition at different positions of the image (1,2,3 and 4).

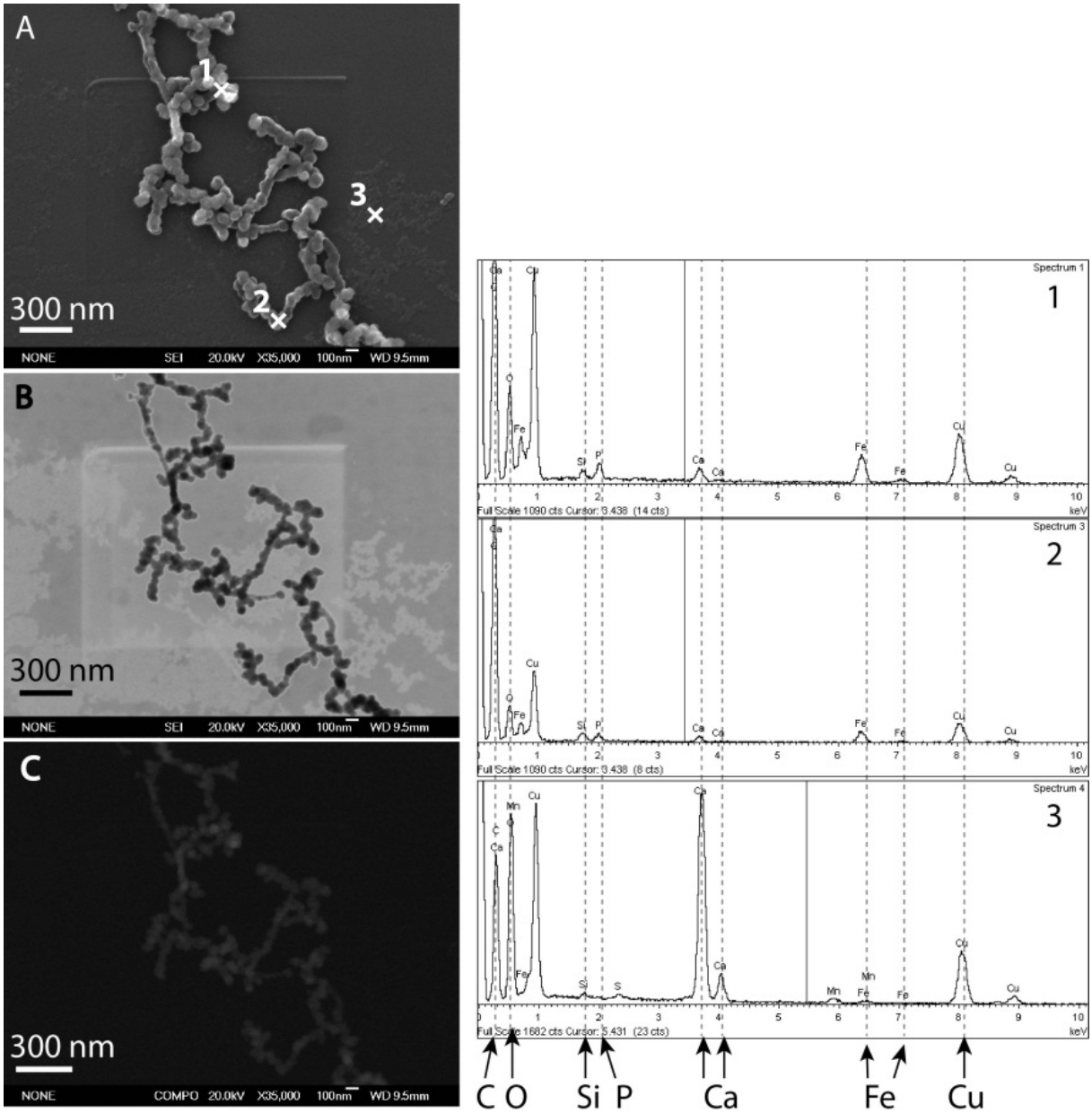

Figure 23 SEM (A), STEM images from secondary electrons (B) and backscattered electrons (C) from sample 28d under sub-oxic conditions taken on February 24th. EDX-spectra showing major element-composition at different positions of the image (1,2,3 and 4).

4.2.4 Field-flow fractionation with UV-absorbance detection

Continuous 0.1-10 nm size distributions of UV-absorbing material, determined by FFF, are shown in Figure. 24. UV-absorbance at 254 nm (UV_{254}) was mainly distributed over the 0.5-6 nm size range, with a maximum at about 1.5 nm. UV-absorbance at 575 nm (UV_{575}) in the sub-oxic samples 26c and 26d had its maximum at a larger size, around 3 nm. UV_{254} showed a secondary maximum, coinciding with the 3 nm maximum in UV_{575}. In the sub-oxic sample 28d, and in the aerated samples, the UV_{575}-signal was too low to be distinsuished from the background. In addition, the peaks in UV_{254} were lower in the aerated samples than in the sub-oxic samples.

It should be noted that the sub-oxic samples analysed by FFF (taken on April 13th were higher in DO (Table 2) than the samples analysed by microscopy (taken on February 24th, Table 2). The material giving rise to a maximum UV_{254} at 1.5 nm is most likely organic matter, e.g., soil fulvic or humic acid. The material giving rise to a 3 nm maximum in UV_{575} behaves in a similar way to

the nanoparticles observed with AFM. For example, the 3 nm UV_{575} maximum was detected in the sub-oxic samples 26c and 26d, but not in the sub-oxic sample 28d, for which AFM determined a broader nanoparticle size distribution, with nanoparticles largely found in the >10 nm size range, e.g., outside the range of FFF. Moreover, the 3 nm UV_{575} maximum could not be observed in the aerated samples, similar to the nanoparticles observed by AFM. However, the size of the UV_{575} maximum determined by FFF (3 nm) was considerably smaller than the size of nanoparticles determined by AFM (about 10 nm). An alternative explanation is that the UV_{575}-maximum at 3 nm represent a different type of organic matter, which is co-aggregated with the nanoparticles when the samples are aerated. Possible compounds include poly aromatic hydrocarbons derived from tannins and lignins (terpinoid precursors) or porphyrin compounds derived from oil or micro-organisms (Leenheer et al., 2003; Lesage et al., 1993), both of which are often associated with landfill leachates.

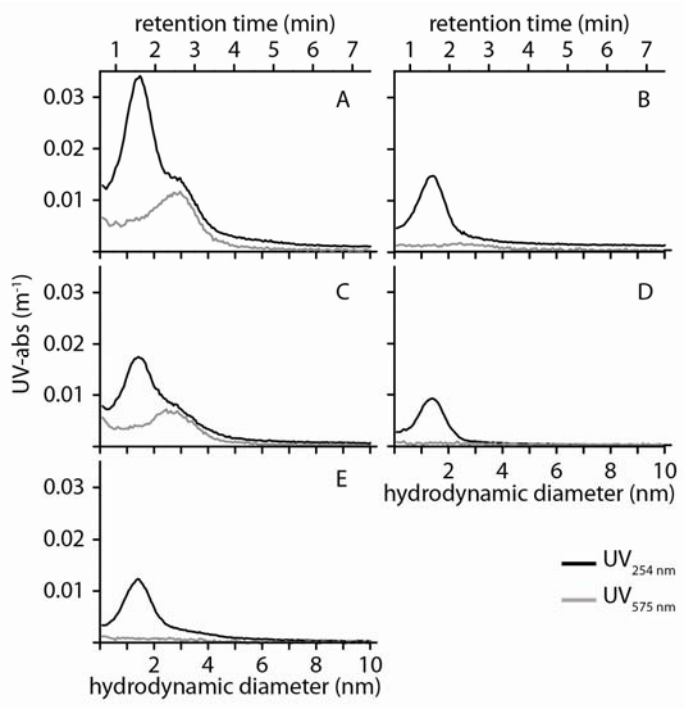

Figure 24 0.5-10 nm FFF size distributions of UV-absorbing material measured at the wavelengths 254 nm and 575 nm, in sample 26c under suboxic conditions (A) and after aeration (B), in sample 26d under sub-oxic conditions (C) and after aeration (D) and in sample 28d under sub-oxic conditions (E). All samples were taken on April 13th.

5 Conclusions

This study has successfully sampled and characterised nano-scale particulate material in sub-oxic groundwaters within an alluvial floodplain aquifer. The integrity of the sample was maintained throughout the field and laboratory work to ensure that nanoparticles representative of the sub-oxic environments were characterised. Nanoparticles from four sites were characterised by multiple methods, AFM, ESEM, TEM and FFF, to explore particle size distributions, morphology and surface chemistry.

These sub-oxic groundwaters were found to have abundant iron and organic nanoparticles with diameters <30 nm. AFM results showed spherical nanoparticles with average diameters of ca 10 nm, while FFF results indicated that smaller fulvic-like nanoparticles were present with average hydrodynamic diameters of ca. 1.5 nm. FFF with UV absorbance detection at 575 nm showed that another population of organic rich nanoparticles were present with larger

hydrodynamic diameters (ca. 3 nm) in the groundwater at nest 26 but were not present in nest 28, perhaps representing aggregated humic-like/Fe rich particles or another source of organic matter.

Fibrillar bipolymeric nano-scale organic material was also observed in sub-oxic samples from nest 28, evidence of the important role of microbiological processes occuring within this leachate plume. It appears that the reductive dissolution of these Fe oxides is progressive down gradient from the landfill, causing a shift in the ratio of dissolved and nanoparticulate Fe. TEM-EDX analysis also showed that Ca rich nanoparticles were present within the groundwater, and that P was associated with the surface of Fe rich particles in nest 28 but not nest 26.

Aeration of sub-oxic samples resulted in a dramatic shift in the nanoparticle size distribution. This was a result of the aggregation of smaller nanoparticles to form larger agglomerations, and the oxidation of Fe (II) to form new nanoparticulate and colloidal Fe oxides, with diameters typically >50-100 nm as observed by AFM. This is analogous to processes that occur during mixing of anaerobic and aerobic environmental waters, e.g. during rapid recharge events, flooding, hyporheic zone mixing, waste water treatment and waste water inputs to surface waters.

Characterising nano-scale particles within these sub-oxic environments is challenging but is critical to understanding pollution attenuation and migration within these systems. Due to their high surface area and rapid transport properties nanoparticles are important vectors for the migration of pollutants such as As, P and NH_4 in the subsurface. Characterising nanoparticles is also important for understanding biogeochemical processes occurring within groundwater bodies impacted by the migration of leachates from waste storage sites. The techniques developed in this study have potential wider applications for understanding the occurrence and fate of natural and anthropogenic (engineered) nanoparticles in sub-oxic conditions.

References

British Geological Survey holds most of the references listed below, and copies may be obtained via the library service subject to copyright legislation (contact libuser@bgs.ac.uk for details). The library catalogue is available at: http://geolib.bgs.ac.uk.

BAALOUSHA, M, AND LEAD JR. 2007. Characterization of Natural Aquatic Colloids (<5 nm) by Flow-Field Flow Fractionation and Atomic Force Microscopy. *Environ. Sci. Technol*., 41 (4), pp 1111–1117. DOI: 10.1021/es061766n

BAALOUSHA, M., V.D.KAMMER, F., MOTELCIA-HEINO,M., HILAL, H, AND COUSTUMER, P. 2006. Size fractionation and characterization of natural colloids by FlFFF-MALLS. *J. Chromatogr*. 1104, 272-281.

BALNOIS E., WILKINSON, K., LEAD, JR, AND BUFFLE, J. 1999. Atomic force microscopy of humic substances: effects of pH and ionic strength. *Envron. Sci. Tech*., 33, 3911-3917.

BACKHUS, DA., RYAN, JN., GROHER, DM., MACFARLANE, JK, AND GSCHWEND, PM. 1993. Sampling Colloids and Colloid-Associated Contaminants in Ground-Water. *Ground Water*, 31, 466-479.

BARGAR, JR, LATMANI-BERNIER, R, GIAMMAR, DE, AND TEBO, BM. 2008. Biogenic uraninite nanoparticles and their importance for uranium remediation. *Elements*, 4(6),407-412;DOI:10.2113/gselements.4.6.407

BUSENBERG, E, AND PLUMMER, LN. 1992. Use of chlorofluorocarbons (CCl3F and CCl2F2) as hydrologic tracers and age-dating tools: The alluvium and terrace system of central Oklahoma, *Water Resour. Res*., 28(9), 2257–2283, doi:10.1029/92WR01263.

CHRISTENSEN, TH., BJERG, PL., BANWART, SA., JAKOBSEN, R., HERON, G, AND ALBRECHTSEN, H-J. 2000. Characterization of redox conditions in groundwater contaminant plumes. *Journal of Contaminant Hydrology*, 45, 165-241.

DEGUELDRE, C., TRIAY, I., KIM, J-IL., VILKS, P., LAAKSPHARJU, AND MIEKELEY, N. 2000. Groundwater colloid properties: a global approach. *Applied Geochem*. 15, 1043-1051.

ELLIOTT, DW, AND ZHANG W. 2001. Field assessment of nanoscale bimetallic particles for groundwater treatment. *Environ. Sci. Technol*., 35 (24), 922–4926, DOI: 10.1021/es0108584.

GIASUDDI., ABM, KANEL, SR, AND CHOI, H. 2007. Adsorption of humic acid onto nanoscale zefovalent iron and its effect on arsenic removal. *Environ. Sci. Technol*. 41, 2022-2027.

GOWING, D, AND YOUNGS E. 2005. The requirements of Apium repens – an ecohydrological assessment. English Nature Final Rep.

GRIFFITHS, K, LAPWORTH DJ, MACDONALD DMJ, STUART M, AND GOODDY DC. 2011. Natural attenuation of anthropogenic groundwater pollution in a peri-urban floodplain setting. Geol. Soc. Conference presentation: Transport and fate of groundwater contaminants, 9th February 2011, London.

GROLIMUND, D, BORKOVEC, M., BARMETTLER, K, AND STICHER, H. 1996. Colloid-facilitated transport of strongly sorbing contaminants in natural porous media: A laboratory colun study. *Environ. Sci. Technol*. 30, 3118-3123.

KLAINE, SJ., ALVAREZ PJJ., BATLEY GE., FERNANDES TF., HANDY RD., LYON DY., MAHENDRA S, MCLAUGHLIN MJ, AND LEAD JR. 2008. Nanomaterials in the environment: Behavior, fate, bioavailability, and effects. *Environmental Toxicology and Chemistry*, 27 (9), 1825–1851.

LAPWORTH DJ., GOODDY, DC., BUTCHER AA, AND MORRIS, BL. 2008. Tracing groundwater flow and sources of organic carbon in sandstone aquifers using fluorescence properties of dissolved organic matter (DOM). *Applied Geochemistry*, 23,3384-3390.

LEAD JR., BALNOIS E., HOSSE M., MENGHETTI R, AND WILKINSON K. 1999. Characterization of Norwegian natural organic matter: size, diffusion coefficients, and electrophoretic mobilities. *Environ Int*., 25:245–58.

LEAD, JR., MUIRHEAD, D, AND GIBSON, CT. 2005. Characterisation of freshwater natural aquatic colloids by atomic force microscopy (AFM). *Environ. Sci. Technol*., 39, 6930-6936.

LEAD, JR, AND WILKINSON KJ. 2006. Aquatic Colloids and Nanoparticles: Current Knowledge and Future Trends. *Environmental Chemistry* 3(3) 159–171, doi:10.1071/EN06025

LEENHEER, JA., NANNY, MA, AND MCINTYRE, C. 2003. Terpenoids as magor precursors of dissolved organic matter in landfill leachates, surface water and groundwater. *Environ. Sci. Technol*., 37 (11), 2323-2331.

LESAGE, S., XU, H, AND DURHAN, L. 1993. The occurrence and roles of porphyrins in the environment: possible implications for bioremediation. *Hydrological Science*, 37 (4), 343-354.

LIANG, L., MCCARTHY JF., JOLLEY LW., MCNABB JA, AND MEHLHORN T.L. 1993. Iron dynamicsobservations of transformation during injection of natural organic matter in a sandy aquifer. *Geochim. Cosmochim. Acta*, 57, 1987-1999.

LIU, Y, MAJETICH SA., TILTON RD., SHOLL DS, AND LOWRY GV. 2005. TCE Dechlorination Rates, Pathways, and Efficiency of Nanoscale Iron Particles with Different Properties. *Environ. Sci. Technol*., 39 (5), 1338–1345, DOI: 10.1021/es049195r

MACDONALD, DM., HALL, R., CARDEN, D., DIXON, A., CHEETHAM, M., CORNICK, S, AND CLEGG, M. 2007. Investigating the interdependencies between surface and groundwater in the Oxford area to help predict the timing and location of groundwater flooding and to optimise flood mitigation measures. Proceedings of 42nd Defra Flood and Coastal Management Conference.

NEWELL AJ. 2007. Morphology and Quaternary geology of the Thames floodplain around Oxford. British Geological Survey Open Report, OR/08/030. 40pp.

REDWOOD PS, LEAD JR, HARRISON RM, JONES IP, AND STOLL S. 2005. Characterisation of humic substances by environmental scanning electron microscopy. . *Environ. Sci. Technol.*, 39,1962-1966.

REINSCH, BC., FORSBERG, B., PENN, RL, AND LOWRY, GV. 2010. Chemical transformations during aging of zerovalent iron nanoparticles in the presence of common groundwater dissolved constituents. *Environ. Sci. Technol*., 44, 3455-3461.

RYAN, JN, AND GSCHWEND, PM. 1990. Colloid mobilisation in two Atlantic coastal plain aquifers: field studies. *Water Resources Research*, 26, 307-322.

RYAN, JN, AND GSCHWEND, PM. 1994a. Effect of Solution Chemistry on Clay Colloid Release from an Iron Oxide-Coated Aquifer Sand. *Environ. Sci. Technol.*, 28, 1717-1726.

RYAN, JN, AND GSCHWEND, PM. 1994b. Effects of Ionic-Strength and Flow-Rate on Colloid Release - Relating Kinetics to Intersurface Potential-Energy. *Journal of Colloid and Interface Science*, Vol. 164, 21-34.

SCHRICK B, HYDUTSKY BW., BLOUGH JL, AND MALLOUK TE. 2004. Delivery Vehicles for Zerovalent Metal Nanoparticles in Soil and Groundwater. *Chem. Mater*., 16 (11), 2187–2193. DOI: 10.1021/cm0218108.

SOHN, K, KANG, SW, AHN, S, WOO, M, AND YANG, S-K. 2006. Fe(0) nanoparticles for nitrate reduction: stability, reactivity and transformation. *Environ. Sci. Technol*., 40, 5514-5519.

SPEELMANS, M, VANTHUYNE, DRJ., LOCK, K., HENDRICKX, F., LAING, G., DU, TRACK, FMG,. AND JANSSEN, CR. 2007. Influence of flooding , salinity and inundation time on the bioavailability of metals in wetlands. *Sci. Tot. Environ*., 380, 144-153 (2007)

UTSUNOMIYA S, KERSTING AB, AND EWING RC. 2009. Groundwater Nanoparticles in the Far-Field at the Nevada Test Site: Mechanism for Radionuclide Transport. *Environ. Sci. Technol*., 2009, 43 (5), pp 1293–1298. DOI: 10.1021/es802181t

WAYCHUNAS GA., KIM CS, AND BANFIELD JF. 2005. Nanoparticulate Iron Oxide Minerals in Soils and Sediments: Unique Properties and Contaminant Scavenging Mechanisms. *Journal of Nanoparticle Research*, 7, (4-5), 409-433, DOI: 10.1007/s11051-005-6931-x

WILKINSON KJ, BALNOIS E, LEPPARD GG, AND BUFFLE J. 1999. Characteristic features of major components of freshwater colloidal organic matter revealed by transmission electron and atomic force microscopy. *Colloids Surf., A*, 155,287-310.

WOLTHOORN, A., TEMMINGHOFF, EJM, AND VAN RIEMSDIJK, WH. 2004b. Colloid formation in groundwater by subsurface aeration: characterisation of the geo-colloids and their counterparts. *Applied Geochemistry*, 19, 1391-1402.

WOLTHOORN, A., TEMMINGHOFF, EJM, WENG, L, AND VAN RIEMSDIJK, WH. 2004a. Colloid formation in groundwater: effect of phosphate, manganese, slilicate and dissolved organic matter on the dynamic heterogeneous oxidation of ferrous iron. *Applied Geochemistry*, 19, 611-622.

ZHANG, W-X., 2003. Nanoscale Iron Particles for Environmental Remediation: An Overview. *Journal of Nanoparticle Research*, 5 (3-4), 323-332, DOI: 10.1023/A:1025520116015.